BLOCKADE OF THE HUMAN ETHER A-GO-GO-RELATED GENE (HERG) POTASSIUM CHANNEL BY FENTANYL

by

Jared Nicholas Tschirhart

A thesis submitted to the Department of Biomedical and Molecular Sciences

In conformity with the requirements for

the degree of Master of Science

Queen's University

Kingston, Ontario, Canada

(June 2019)

Abstract

Fentanyl poses a serious health concern, with abuse and death rates rising over recent years. Despite the high number of overdose deaths attributed to fentanyl, the complete molecular mechanisms of such deaths have not been well-defined. Although activation of opioid receptors in the brainstem causes respiratory depression, in most cases of drug-induced sudden death cardiac arrhythmias are implicated. Therefore, we posited that disruption of cardiac electrophysiology may contribute to fentanyl-induced death. The *human ether-a-go-go-related gene* (*hERG*) encodes the pore-forming subunit of the rapidly activating delayed rectifier potassium channel (I_{Kr}). Drug-mediated disruption of hERG function is the primary cause of acquired long QT syndrome, which predisposes affected individuals to ventricular arrhythmias and sudden death. Therefore, we investigated the effects of fentanyl on hERG channels. The effects of norfentanyl, the main metabolite, and naloxone, an antidote used in fentanyl overdose, were also examined. Currents of hERG channels stably expressed in HEK293 cells were recorded using whole-cell voltage-clamp. When hERG tail currents upon −50 mV repolarization after a 50 mV depolarization were analyzed, fentanyl and naloxone blocked hERG current (I_{hERG}) with IC_{50} values of 0.9 and 74.3 μM, respectively, whereas norfentanyl did not block. The reduction of I_{hERG} by fentanyl was not antagonized by naloxone, indicating that the reduction was not through activation of opioid receptors. An interesting finding is that fentanyl-mediated block of I_{hERG} was voltage-dependent. Consequently, when a human ventricular action potential waveform voltage protocol was used, fentanyl blocked I_{hERG} with an IC_{50} of 0.3 μM, which is within the range of blood concentrations after overdose deaths in humans. Furthermore, fentanyl (0.5 μM) blocked I_{Kr} and prolonged action potential duration in ventricular myocytes isolated from neonatal rats. The concentrations of fentanyl used in this project were higher than seen with

clinical use but overlap with post-mortem overdose concentrations. Further, co-expressed long and short isoforms of hERG, proposed to mimic native channels, displayed an increased sensitivity to fentanyl. Although mechanisms of fentanyl-related sudden death need further investigation, blockade of hERG channels may contribute to death for individuals with high-concentration overdose or compromised cardiac repolarization.

Co-Authorship

Shetuan Zhang and I conceptualized the project. I designed experiments with the assistance of Shetuan Zhang, Wentao Li, and Jun Guo. Jun Guo performed cell culture and neonatal rat ventricular myocyte isolations. I collected all Western blot data. Electrophysiology results were collected by Jun Guo, Wentao Li, and I. For figures 6-14 and 16, my contributions were varied. Generally, I collected at least 50% of data, with details in the legends of select figures. For figures 15, and 17-20 I collected all data.

Acknowledgements

This project would not have been possible without the wealth of direct and indirect support that I have received over the last two years. First of all, I would like to thank my supervisor, Dr. Shetuan Zhang for his ongoing help and confidence. Through our interactions I have learned a lot about science, professionalism, and life. I would also like to thank Jun Guo and Wentao Li for the time and patience they dedicated to teaching laboratory techniques, particularly patch clamp. Your assistance in this project was indispensable. I would also like to acknowledge the other members of the Zhang lab throughout my time here: Tonghua Yang, Dr. Shawn Lamothe, Jordan Davis, Morgan Sutherland-Deveen, Alex Milton, Nancy You, Dr. Tingzhong Wang, Dr. Yuan Du, Mark Szendry, and Taylore Dodd. Thank-you for making this Master's an enjoyable experience. I am grateful for the friendships forged, the opportunities for out-of-lab activities, and the extracurriculars that made these two years enjoyable. A particular thank-you to Dr. Shawn Lamothe, who served as a mentor when I arrived in the lab. With your guidance and assistance, I have grown as a scientist and a person.

I also owe an acknowledgement to the many wonderful faculty members I have interacted with. Firstly, my supervisory committee, Dr. Neil Magoski and Dr. Don Maurice, thank-you for your time and helpful suggestions. Also, thank-you to the faculty involved with LISC391 for teaching me so much about teaching and making my several terms as a teaching assistant enjoyable.

Last but not least, I would like to thank my family and my significant other, Paityn Major, for supporting me in my academic career, keeping me grounded, and helping me navigate the difficult life decisions. Without your support, I would not be where I am today.

Table of Contents

List of Figures

List of Abbreviations

AP	action potential
ANOVA	analysis of variance
APD	action potential duration
APD_{90}	action potential duration at 90% repolarization
CNBD	cyclic nucleotide binding domain
CTL	control
DF	Dulbecco's modified eagle medium/F12
DNase	deoxyribonuclease
EAG	ether-a-go-go
ECG	electrocardiogram
ER	endoplasmic reticulum
FBS	fetal bovine serum
HCN	hyperpolarization activated cyclic nucleotide gated
HEK	human embryonic kidney
hERG	human ether-a-go-go-related gene
IC_{50}	half maximal inhibitory concentration
I_f	pacemaker or "funny" current
I_{hERG}	hERG current
I_{KAch}	G-protein-activated K^+ current
I_{Kr}	rapidly activating delayed rectifier potassium current
I_{Ks}	slowly activating delayed rectifier potassium current
I_{Na}	sodium current

I_{to}	transient outward potassium current
KCNE1	potassium voltage-gated channel subfamily E regulatory subunit 1
KCNE2	potassium voltage-gated channel subfamily E regulatory subunit 2
LJP	liquid junction potential
LQTS	long QT syndrome
MEM	minimum essential medium
MinK	minimal potassium channel subunit
MiRP1	MinK-related peptide 1
NRVMs	neonatal rat ventricular myocytes
HRP	horseradish peroxidase
PAS	Per-Arnt-Sim
PBS	phosphate buffered saline
S.D.	standard deviation
SDS	sodium dodecyl sulfate
τ_{inact}	time constant of inactivation
$\tau_{f\text{-}deact}$	fast time constant of deactivation
$\tau_{s\text{-}deact}$	slow time constant of deactivation
TCC	tetramerizing coiled coil
TdP	torsade de pointes
$V_{1/2}$	voltage of half- maximal activation
VSD	voltage sensor domain
WT	wild-type

Chapter 1

Introduction and Literature Review

1.1 Fentanyl

In recent years, fentanyl-associated death has become a serious issue in North America. In fact, within British Columbia, there were 1,310 fentanyl-detected illicit drug overdose deaths reported in 2018 alone (BC Coroners Service, 2019). Further, fentanyl was detected in 87% of all illicit drug deaths during 2018 (BC Coroners Service, 2019). Fentanyl is a potent synthetic opioid that acts as a μ-opioid receptor agonist (Raynor *et al.*, 1994). The affinity of fentanyl for the μ-receptor is 150 and 242 times greater than for the δ- and κ-opioid receptors, respectively (Maguire *et al.*, 1992). Fentanyl is used clinically for management of severe pain and combined with other drugs for anesthesia (Stanley, 2014). Illicit fentanyl use poses a risk because of its addictive characteristics and side effects, particularly its propensity to cause sudden death. The medulla oblongata of the brainstem contains a high density of opioid receptors (Wamsley, 1983). It is known that fentanyl acts at these receptors, which causes a reduction in chemosensitivity to hypercapnia and hypoxia, diminishing respiratory drive from the central nervous system (McQueen, 1983). This fentanyl-induced respiratory depression is believed to underlie fentanyl-induced sudden death. However, in many cases of sudden death, disruption of cardiac electrophysiology is implicated (Roden, 2004).

Fentanyl is highly lipophilic and distributes quickly and extensively from plasma to bodily compartments such as the central nervous system (Hug & Murphy, 1979). In humans, the volume of distribution is approximately 310 L (4.08 L/kg) (McClain & Hug, 1980). After an intravenous dose, over 95% of a dose is eliminated from the plasma in the first 5 minutes, mostly

through uptake to the brain, heart and lung, followed by uptake to skeletal muscle and fat with a slower time course (Murphy *et al.*, 1979; Hug & Murphy, 1979, 1981; McClain & Hug, 1980). Notably, a study in rats found that heart tissue concentrations of fentanyl are 2-3 times higher than plasma after this redistribution (Hug & Murphy, 1981). In humans, post-mortem heart tissue concentrations after overdose were 1.9-5.4 times greater than femoral blood concentrations (Luckenbill *et al.*, 2008); however, in this study there was a delay between death and analysis, so post-mortem fentanyl redistribution should not be ruled out. A larger study found that post-mortem heart tissue fentanyl concentrations at autopsy were an average of 6 times greater than heart blood at autopsy, 6 times greater than femoral blood at autopsy, and 38 times greater than femoral blood shortly after death (2.5- 6 hours) (Olson *et al.*, 2010). However, once again, post-mortem redistribution of fentanyl may play a role in the higher heart concentrations observed in this study.

Fentanyl is rapidly metabolized by hepatic biotransformation to allow for excretion, as less than 8% of intravenous fentanyl is excreted unchanged in urine and stool (McClain & Hug, 1980; Bovill & Sebel, 1980; Tanaka *et al.*, 2014). The major route of metabolism is N-dealkylation by cytochrome P450 3A4 to form norfentanyl (Goromaru *et al.*, 1984; Tateishi *et al.*, 1996). Other metabolites have been found, including despropionylfentanyl (Van Rooy *et al.*, 1981), hydroxyfentanyl (Goromaru *et al.*, 1984), and hydroxynorfentanyl (Goromaru *et al.*, 1984); however, these metabolites are minor compared to norfentanyl and are not reliably detected. Such fentanyl metabolites, including norfentanyl, do not demonstrate significant activity at opioid receptors (Schneider & Brune, 1986), and thus the duration of effect is dependent on the time required to metabolize fentanyl. After the initial fast decrease in plasma fentanyl concentrations arising from uptake into tissues, clearance occurs through two phases.

The first phase is the metabolism of fentanyl from the central compartment, and this occurs with a relatively fast time constant of 13.4 min in humans (McClain & Hug, 1980). The central compartment includes the lung, heart, brain, and liver, where exchange of fentanyl occurs readily and elimination of fentanyl parallels its elimination from plasma, despite differences in absolute concentrations (Hug & Murphy, 1979, 1981). The second phase of elimination is rate limited by the reuptake of fentanyl from the peripheral compartment tissues to the central compartment and plasma, where it can be metabolized in the liver; the time constant of this slower phase is 219 minutes in humans (McClain & Hug, 1980). The peripheral compartment tissues include skeletal muscle and fat (Hug & Murphy, 1981). Thus, despite fast clearance from the plasma, there is a slow release of unmetabolized fentanyl from the peripheral compartment, leading to prolonged clearance and accumulation in the body with repetitive doses (Murphy *et al.*, 1979).

The drug commonly used for reversing fentanyl overdose is naloxone. Naloxone is a competitive inhibitor of μ-, δ- and κ-opioid receptors (Martin, 1976). Therefore, when given during a fentanyl overdose, it prevents binding to the μ-opioid receptor and displaces fentanyl from occupied receptors (Villiger *et al.*, 1983). The efficacy of naloxone for reversing fentanyl overdose is high, and it is effective in preventing death (Clark *et al.*, 2014; Rzasa Lynn & Galinkin, 2018); however, there are cases of atrial and ventricular arrhythmias (Michaelis *et al.*, 1974; Azar & Turndorf, 1979; Cuss *et al.*, 1984; Merigian, 1993; Hunter, 2005; Lameijer *et al.*, 2014) and sudden death (Andree, 1980) following naloxone administration for opioid overdose treatment or reversal of surgical anesthesia.

1.2 The Cardiac Action Potential

The normal synchronous heart rhythm is controlled by a balanced flow of ions such as Na^+, Ca^{2+} and K^+ into and out of cardiomyocytes through ion channels. Such currents give rise to

cardiac action potentials (APs). Cardiac APs are stimulated by autorhythmic cells located within the sinoatrial node of the right atrium. The autorhythmic activity of these cells arises from hyperpolarization activated cyclic nucleotide gated (HCN) channels, transient (T-type) Ca^{2+} channels, and heterotetrametric Kir3.1 and Kir3.4 channels, which generate G-protein-activated K^+ current (I_{KAch}). HCN channels generate cardiac pacemaker or funny current (I_f), and are activated by intracellular cAMP or hyperpolarization, with a voltage of half-maximal activation ($V_{1/2}$) around −60 to −70 mV (Baruscotti *et al.*, 2005). HCN channels have a mixed permeability of Na^+ and K^+, generating a net depolarizing current when activated at hyperpolarized potentials (Baruscotti *et al.*, 2005). Upon reaching threshold potential, a cardiac AP is evoked.

The cardiac AP occurs in five phases; for the purposes of this thesis, the ventricular AP will be of focus (Fig. 1). During phase 4, non-autorhythmic ventricular myocytes are at resting membrane potential, approximately −90 mV. Resting membrane potential is primarily maintained by I_{K1}, an inward rectifying potassium current that is activated at hyperpolarized potentials (Deal *et al.*, 1996). During phase 0, membrane depolarization activates sodium channels, giving rise to inward Na^+ current (I_{Na}), which results in membrane depolarization. Phase 1 is characterized by a notch in the membrane potential, caused by an early transient repolarization arising from transient outward potassium current (I_{to}) (Deal *et al.*, 1996). Phase 2 is the plateau, where the repolarizing effect of I_{to} is offset by inward L-type calcium current ($I_{Ca(L)}$), resulting in a relatively stable membrane potential. Phase 3 is the repolarization phase. The repolarization phase begins with the activation of KCNQ1 channels, which pass the slowly activating delayed rectifier potassium current (I_{Ks}) and the closure of L-type calcium channels. The corresponding negative change in membrane potential opens human ether-a-go-go-related gene (hERG) potassium channels to pass the rapidly activating delayed rectifier potassium

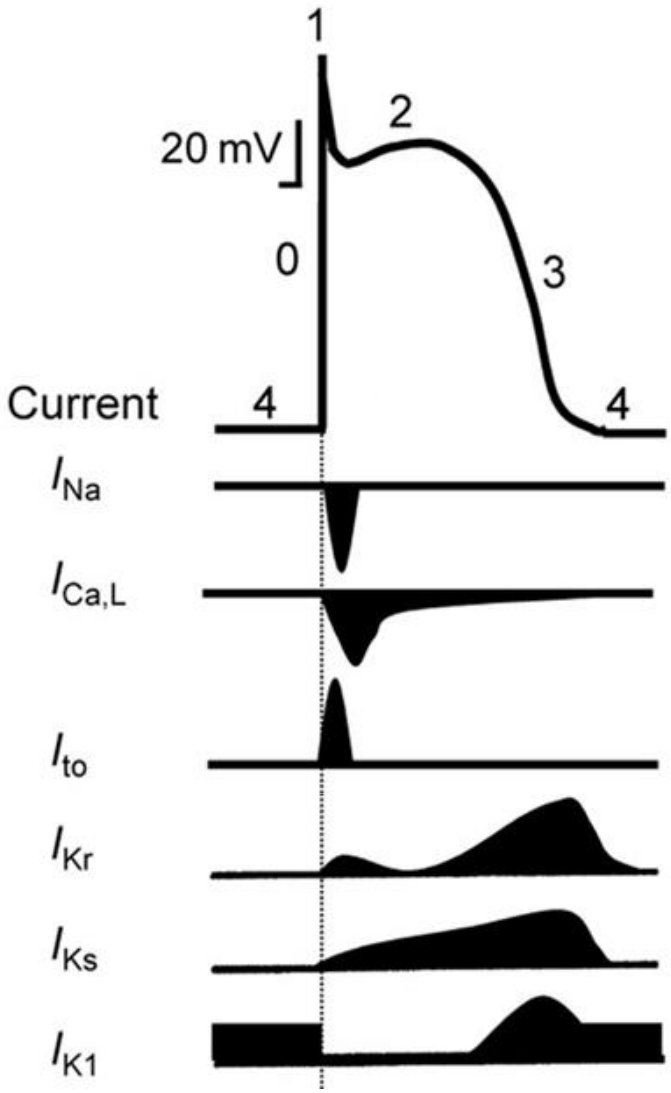

Figure 1. Human ventricular action potential and the corresponding currents.

This diagram of membrane voltage represents a cardiac AP in a non-autorhythmic ventricular myocyte. During phase 4, the resting membrane potential is primarily maintained by I_{K1}. Phase 0 is commenced when exogenous stimulation depolarizes the membrane, activating I_{Na}. In phase 1, I_{Na} inactivates, and the membrane is slightly repolarized by I_{to}. During phase 2, $I_{Ca(L)}$ maintains the membrane at a relatively constant potential, called the plateau. Phase 3 is characterized by the repolarization of the membrane by I_{Ks} in the early stage, and later by I_{Kr}. Figure modified from Moreno *et al.* (2012).

current (I_{Kr}). These currents drive the membrane back to resting potential (phase 4). Thus, I_{Kr} is critical for phase 3 repolarization of the cardiac AP and participates in determining action potential duration (APD) (Curran *et al.*, 1995; Sanguinetti *et al.*, 1995; Keating & Sanguinetti, 2001).

1.3 The hERG K^+ Channel and Long QT Syndrome

1.3.1 Structure and Function

hERG encodes the pore-forming α-subunit of the hERG potassium channel (Warmke & Ganetzky, 1994; Curran *et al.*, 1995), which generates I_{Kr} (Sanguinetti *et al.*, 1995; Trudeau *et al.*, 1995). The hERG α-subunit is made up of several domains. The Per-Arnt-Sim (PAS) domain constitutes the first 135 residues of the N-terminus (Cabral *et al.*, 1998). The PAS domain in question is highly conserved amongst the ether-a-go-go (EAG) K^+ channel family (Warmke & Ganetzky, 1994). The PAS domain is important for regulating hERG channel gating, particularly deactivation. It was found that deletion of most (residues 2-354) (Spector *et al.*, 1996*b*; Wang *et al.*, 1998) or all (residues 2-373) (Schönherr & Heinemann, 1996) of the N-terminus removes slow deactivation, decreasing the deactivation time constants. More specifically, deletion of the PAS domain (Cabral *et al.*, 1998) but not the proximal N-terminus (residues 138-373) (Viloria *et al.*, 2000) decreases deactivation time constants, suggesting that the PAS domain is critical for slow deactivation kinetics. Cabral *et al.* (1998) discovered a hydrophobic patch on the surface of the PAS domain and proposed that this patch forms strong interactions with the body of the channel to slow deactivation rates. Mutational analyses unveiled that the PAS domain interacts with the cyclic nucleotide binding domain (CNBD) of the channel to regulate deactivation kinetics (Gustina & Trudeau, 2011) through interaction between positively charged residues in the PAS domain and negatively charged residues in the CNBD (Ng *et al.*, 2014). The CNBD is

located within the C-terminus of the hERG channel. In addition to its role in determining deactivation kinetics, the CNBD is important for channel trafficking to the membrane, as mutations in this region prevent Golgi transit and cause retention of channels in the ER (Akhavan *et al.*, 2003, 2005). In addition to the CNBD, the C-terminus of hERG contains a tetramerizing coiled coil (TCC) domain. As the name suggests, these domains form coiled-coil structures, which interact to form tetramers that are important for the assembly of functional channels (Jenke *et al.*, 2003). Between the N- and C-termini, the hERG α-subunit consists of six transmembrane segments (S1-S6). The voltage sensor domain (VSD) is made up of S1-S4, while the pore domain is comprised by S5 and S6, forming the ion conduction pathway in the tetrameric channel (Fig. 2) (Vandenberg *et al.*, 2012).

Two main isoforms of the hERG α-subunit exist (Fig. 3): it was originally believed that only the 1a transcript of the *hERG* gene encoded for α-subunits; however, an alternate transcript termed 1b was uncovered and further characterized over several years (Lees-Miller *et al.*, 1997; London *et al.*, 1997; Jones *et al.*, 2004; Phartiyal *et al.*, 2007). The hERG 1a isoform is 1159 amino acids in length (Warmke & Ganetzky, 1994) and contains the domains described. The shorter 1b isoform was first cloned from mouse heart cDNA. It is 820 amino acids long, and although S1 to the C-terminus is identical to hERG 1a, hERG 1b contains a unique, shorter (36 amino acid long) cytoplasmic N-terminus (Lees-Miller *et al.*, 1997; London *et al.*, 1997) and lacks the PAS domain. Interestingly, when hERG 1a and 1b are co-expressed in heterologous expression systems, the currents resemble native I_{Kr} more closely than hERG 1a expressed alone (London *et al.*, 1997; Sale *et al.*, 2008; Larsen & Olesen, 2010), indicating that both contribute to the native current. The presence of the hERG 1b subunit was further supported by detection on Western blots of isolated human and canine ventricular myocyte membrane proteins

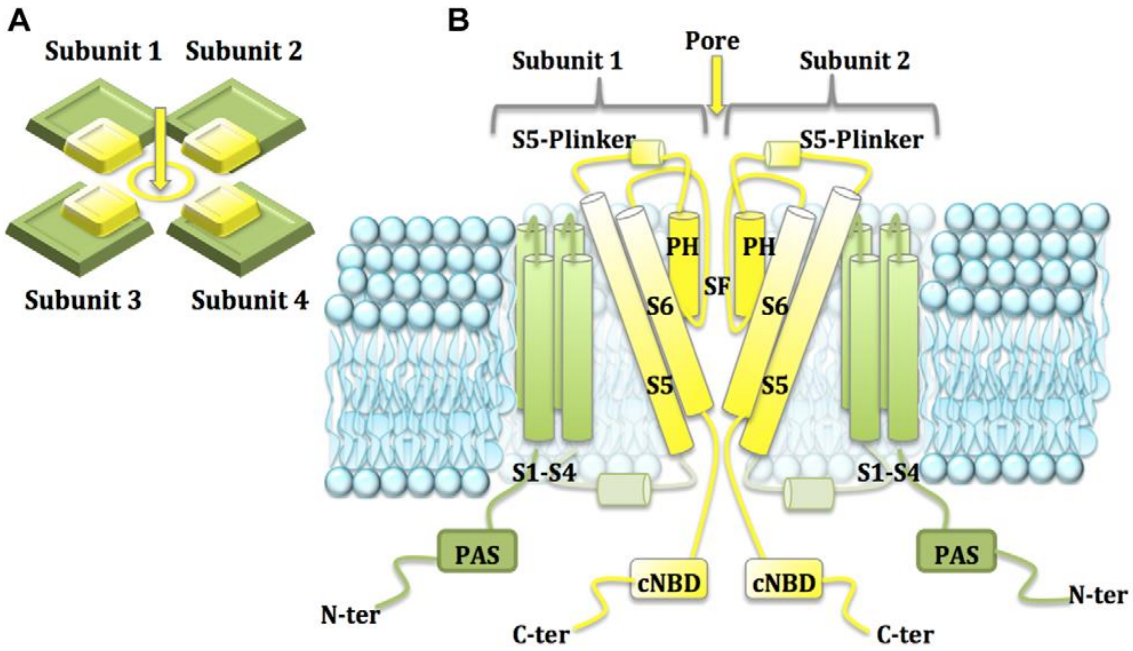

Figure 2. Kv11.1 channel structure.

(A) Four hERG α-subunits assemble to form channels, with the ion-conducting pore located in the center. (B) Schematic of an assembled channel in the plasma membrane. Only two subunits are shown for clarity. The N-terminal tail (N-ter) and C-terminal tail (C-ter), including the Per-Arnt-Sim (PAS) domain and cyclic nucleotide binding domain (CNBD) respectively, are located intracellularly. The transmembrane segments S1-S6 are located in the plasma membrane. The voltage sensing domain (VSD) is formed by S1-S4 and the pore is formed by S5 and S6. The pore helix (PH) stabilizes the inactivation gate of the channel, whereas the selectivity filter (SF) confers selectivity to the conductance of K^+. Figure modified from Kalyaanamoorthy & Barakat (2018).

(Jones *et al.*, 2004). Co-immunoprecipitation analyses demonstrated that hERG 1a and 1b subunits co-assemble to form heterotetramers within the endoplasmic reticulum (ER) as channels become associated after core glycosylation, which occurs co-translationally in the ER, but before complex glycosylation, which occurs in the Golgi apparatus (Jones *et al.*, 2004; Phartiyal *et al.*, 2007). Finally, the functional role of hERG 1b was elucidated using human induced pluripotent stem cell-cardiomyocytes, in which knockdown of hERG 1b with short hairpin RNA decreases I_{Kr}, prolongs APD, and increases APD variability (Jones *et al.*, 2014). As the discovery of the hERG 1b transcript was relatively recent, the hERG-HEK cell line used for the majority of this project contains solely hERG 1a, in line with most current research.

When fully assembled, channels form a heterotetramer of 1a and 1b α-subunits, through interactions between the TCC domains of individual subunits. Fully assembled channels are sometimes referred to as Kv11.1, or commonly hERG channels. Further, channels associate with up to two transmembrane accessory β-subunits. The subunits in question are potassium voltage-gated channel subfamily E regulatory subunit 1 (KCNE1) also known as minimal potassium channel subunit (MinK), and potassium voltage-gated channel subfamily E regulatory subunit 2 (KCNE2) also known as MinK-related peptide 1 (MiRP1). MinK (McDonald *et al.*, 1997; Finley *et al.*, 2002) and MiRP1 (Abbott *et al.*, 1999; Mazhari *et al.*, 2001) have been shown to associate with hERG channels and alter channel gating and current density. However, the role of β-subunits in vivo is still under debate as expression of these subunits is not essential for generation of hERG current in heterologous expression systems (Anantharam & Abbott, 2005; Li *et al.*, 2006; Abbott *et al.*, 2007; Vandenberg *et al.*, 2012), in contrast to KCNQ1, which requires co-expression of MinK to generate current (Barhanin *et al.*, 1996; Sanguinetti *et al.*, 1996).

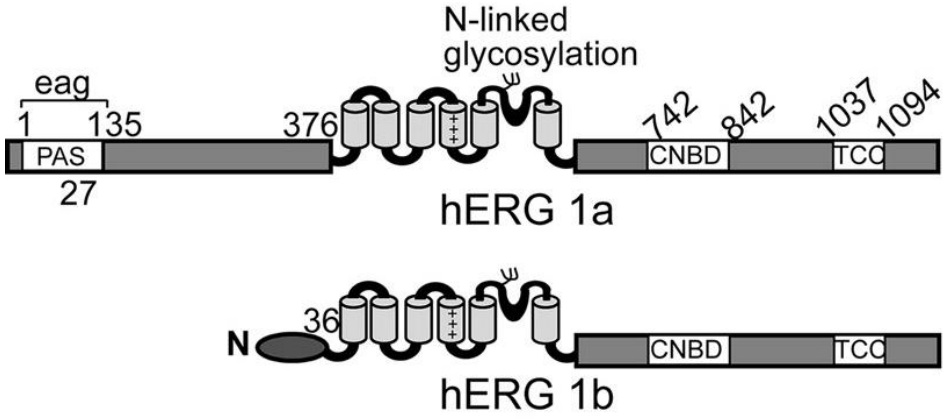

Figure 3. hERG 1a and 1b isoforms.

A diagrammatic representation of the hERG 1a isoform (expressed in the hERG-HEK cell line used for the majority of this project) and the shorter hERG 1b isoform. hERG 1b is identical to 1a from position 376 onward. However, it is lacking residues 1-375 and contains a unique, 36 amino acid long N-terminal region located intracellularly. Also illustrated are the major domains. The N and C-termini are represented by grey boxes, transmembrane segments by grey cylinders, linkers by black lines, and domains by white boxes. Figure modified from Phartiyal *et al.* (2007).

1.3.2 Gating and Kinetics

The hERG channel exhibits some unique gating properties. The channel can exist in closed (deactivated), open (activated), or inactive states (Fig. 4A), with current being passed only when the channel is in the open state. At resting potential channels are closed. Upon membrane depolarization, the channels first activate. The time course of activation is faster than KCNQ1 (I_{Ks}) channels, and thus current passed by hERG is referred to as I_{Kr}, despite the activation time course being slower than some other channel types, such as sodium channels. The channels then undergo C-type inactivation, where the conformation of the channel pore is altered, preventing the passage of potassium ions (Schönherr & Heinemann, 1996). hERG channnel inactivation is voltage-dependent, with a greater degree of inactivation and faster time course at more positive membrane potentials (Smith *et al.*, 1996; Spector *et al.*, 1996*b*; Schönherr & Heinemann, 1996). This phenomenon gives rise to the inward rectification properties of hERG channels, as outward current at membrane potentials positive to the reversal potential is diminished by more extensive inactivation, whereas inactivation is minimal at potentials negative to the reversal potential. Additionally, inactivation of hERG channels occurs with a very fast time course, faster in fact than activation (Sanguinetti *et al.*, 1995; Trudeau *et al.*, 1995; Smith *et al.*, 1996). Therefore, the current passed upon initial depolarization is small given the driving force (Fig. 4B) as a large portion of channels are inactivated. Upon repolarization, hERG channels rapidly transition from the inactive to open state, giving rise to a characteristic 'hook' or 'tail current', which represents open channel conductance in response to the preceding depolarization (Fig. 4B). After recovery from inactivation, the channels slowly transition from the open state to the closed state, which is a two-step process best fit with a biexponential function (Sanguinetti *et al.*, 1995; Trudeau *et al.*, 1995). As such, deactivation proceeds with two time constants, one fast and one slow. At more

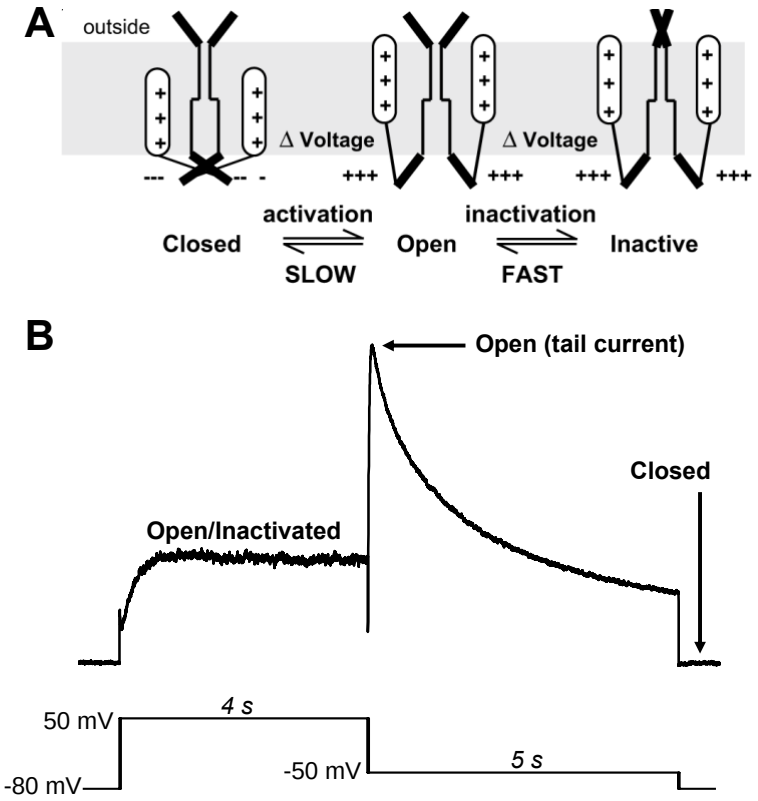

Figure 4. hERG channel states and a demonstration of I_{hERG}.

(A) hERG channels can exist in closed (deactivated), open (activated), or inactive states. The transition from closed to open and vice versa is slow, whereas the transition from open to inactive and vice versa is fast. Figure modified from Perrin *et al.* (2008). (B) Current trace (top) recorded from a hERG-HEK cell expressing hERG 1a in response to the shown voltage protocol (bottom). Upon initial depolarization to +50 mV, the majority of channels activate. However, during the course of channel activation, a large proportion of channels quickly inactivate due to voltage-dependent inactivation. Upon repolarization to –50 mV, the inactivated channels quickly recover to the open state, giving rise to tail current before slowly deactivating. Therefore, tail current represents maximal channel conductance when given an adequate depolarization such as +50 mV and can also be used to determine the proportion of channels activated by a given depolarizing pulse when activation is less than maximal.

positive potentials (above –60 mV) the slow component predominates, whereas at voltages negative to –60 mV the fast component predominates (Vandenberg *et al.*, 2006).

The N-terminus of hERG influences several gating properties. Deletion of the majority of the N-terminus (residues 2-354 or 373) of hERG shifts the voltage-dependence of activation and inactivation by 20 to 30 mV in the positive direction, and drastically accelerates deactivation (Spector *et al.*, 1996*b*; Schönherr & Heinemann, 1996). As discussed, interactions between the PAS and CNDB are believed to underlie the role of the N-terminus in hERG deactivation (Gustina & Trudeau, 2011). These altered kinetics are of interest as heterologously expressed hERG 1a and 1b heterotetramers display similar properties. Sale *et al.* (2008) found that heterotetrameric channels demonstrate larger current amplitude, accelerated activation, positively shifted voltage-dependence of inactivation, accelerated recovery from inactivation, and accelerated deactivation compared to homotetrameric hERG 1a channels expressed in HEK293 cells. It has been proposed that the presence of 1b subunits explains the differences in observed gating kinetics between heterologously expressed hERG 1a and I_{Kr} recorded from ventricular myocytes (Mitcheson & Hancox, 1999; Weerapura *et al.*, 2002).

1.3.3 Drug Block, Long QT Syndrome, and Sudden Death

A decrease in hERG channel function prolongs APD, which manifests as long QT syndrome (LQTS), a prolongation of the QT interval on a surface ECG recording (Fig. 5). Notably, LQTS predisposes affected individuals to a polymorphic ventricular tachycardia known as Torsade de Pointes (TdP, Fig. 5) (Keating and Sanguinetti, 2001). TdP arises from prolonged repolarization due to reactivation of L-type calcium channels, which can trigger a premature

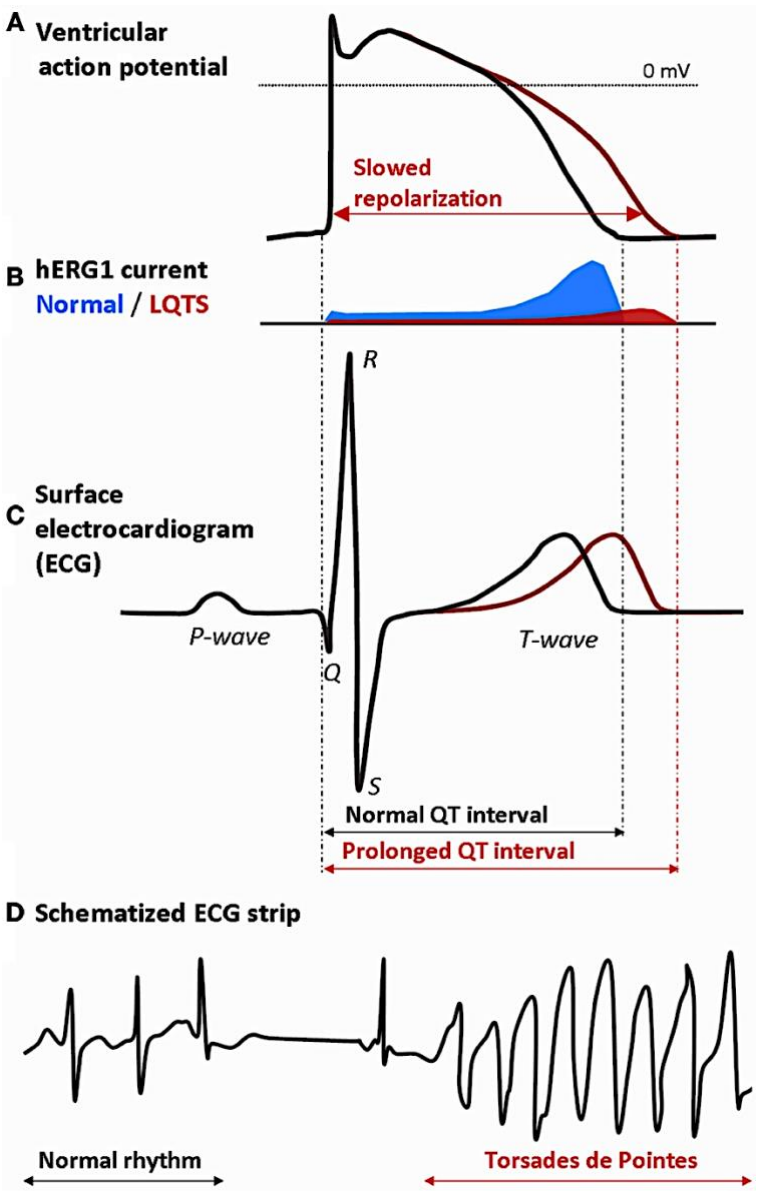

Figure 5. QT prolongation arising from decreased hERG function.

(A) A ventricular AP in the normal situation (black line) and in LQTS (red). (B) hERG current is usually maximal near the end of phase 3 repolarization (blue), but peak current is decreased in LQTS (red). (C) A representation of how electrical activity in cardiomyocytes gives rise to a surface ECG recording, and the effect of a prolonged repolarization phase. (D) A prolonged QT interval can cause a premature ventricular depolarization referred to as an early after depolarization. This premature depolarization triggers TdP, which can eventually degenerate into ventricular fibrillation and sudden death. Figure modified from Grilo *et al.* (2010).

ventricular depolarization known as an early after depolarization (Shimizu *et al.*, 1995; Chiang & Roden, 2000). TdP may resolve spontaneously, but can degenerate into ventricular fibrillation leading to sudden death (Chiang & Roden, 2000).

1.4 Hypothesis and Objectives

It is unclear if cardiac arrhythmias play a role in fentanyl-related deaths. Although synthetic opioids such as methadone (Kornick et al., 2003; Krantz et al., 2003; Maremmani et al., 2005; Martell et al., 2005) have been observed to prolong the QT interval in humans, the clinical literature regarding fentanyl is less clear; unchanged (Chang *et al.*, 2008; Cafiero *et al.*, 2011; Hancı *et al.*, 2013; Öztürk *et al.*, 2015) and prolonged (Lischke *et al.*, 1994; Keller *et al.*, 2016; Cho *et al.*, 2016; Xuan *et al.*, 2018) QT intervals have been reported. These discrepancies may be due to the design of these studies, as low doses of fentanyl in combination with other anaesthetic agents were used in most cases. A recent review suggests a dose-dependent effect of fentanyl on the QT interval (Behzadi *et al.*, 2018), though the mechanism remains elusive. Experimentally, fentanyl at concentrations of 94.6 nM, 190 nM, and 950 nM prolong the cardiac AP in isolated canine ventricular Purkinje fibers (Blair *et al*., 1989). As the prolongation is not reversed by naloxone, the authors proposed that it arose from a mechanism separate from μ-opioid receptor agonism (Blair *et al*., 1989). Since the reduction of I_{Kr} prolongs AP duration and is responsible for most cases of drug-induced LQTS, we investigated the effects of fentanyl on hERG 1a channels stably expressed in HEK293 (hERG-HEK) cells. We also examined the effects of fentanyl on cardiac APs and various currents in neonatal rat ventricular myocytes (NRVMs). Furthermore, the effects of norfentanyl were studied to determine if the metabolic product of fentanyl could contribute to sudden death. As naloxone has been shown to induce cardiac arrhythmias in some individuals, it was also examined. I hypothesized that fentanyl,

norfentanyl, or naloxone decrease I_{hERG} and I_{Kr}, leading to prolongation of APD. To address this hypothesis, I examined the chronic effects of fentanyl, norfentanyl, and naloxone on hERG membrane protein in hERG-HEK cells using Western blot analysis. To examine the acute effects of fentanyl, norfentanyl, and naloxone on I_{hERG} and I_{Kr}, I used whole-cell voltage-clamp on hERG-HEK cells and isolated NRVMs, respectively. Lastly, to observe effects on APD, APs were recorded from isolated NRVMs using whole-cell current-clamp. Further, the mechanism of fentanyl block as well as the physiologic relevance were further examined using whole-cell voltage-clamp recordings from hERG-HEK cells.

Chapter 2

Materials and Methods

2.1 Molecular Biology

hERG cDNA was provided by Dr. Gail Robertson (University of Wisconsin-Madison, Madison, WI). Point mutations Y652A, F656T, S631A, S620T, and S620C were created using polymerase chain reaction overlap extension technique, as described previously (Guo *et al.*, 2006). The Δ2-354 and Δ2-9 hERG mutants were also created using the PCR method and confirmed by DNA sequencing (GENEWIZ, South Plainfield, NJ). Human EAG cDNA was provided by Dr. Luis Pardo (Max-Planck Institute of Experimental Medicine, Göttingen, Germany). Human Kv1.5 cDNA was provided by Dr. Michael Tamkun (Colorado State University, Fort Collins, CO). Human KCNQ1 and KCNE1 cDNAs were provided by Dr. Michael Sanguinetti (University of Utah, Salt Lake City, UT). Human Kv4.3 was provided by Gui-Rong Li (University of Hong Kong, Hong Kong, Hong Kong Special Administrative Region of the People's Republic of China). Human Kir2.3 cDNA was provided by Dr. Carol Vandenberg (University of California, Santa Barbara, Santa Barbara, CA). The HEK293 cell line stably expressing wild-type (WT) hERG channels (hERG-HEK cell line) was obtained from Dr. Craig January (University of Wisconsin-Madison). HEK293 cell lines stably expressing Δ2-354 hERG, EAG, Kv1.5, and KCNQ1 + KCNE1 were created using transfection followed by G418 selection (1 mg/mL) and maintenance (0.4 mg/mL). Kv4.3, Kir2.3, and mutant hERG Y652A, F656T, S631A, S620C, S620T, and Δ2-9 were transiently expressed in HEK293 cells. For transient transfection, GFP cDNA [pIRES2-EGFP (enhance GFP); Takara Bio USA, Inc., Mountain View, CA] was co-transfected for the selection of transfected cells during patch-clamp experiments. For co-

expression of WT and Δ2-354 hERG, 2 μg of each plasmid were mixed and transfected together with GFP. HEK293 cells were cultured in Gibco minimum essential medium (MEM) consisting of calcium chloride ($CaCl_2$), choline chloride, D-calcium pantothenate, folic acid, L-arginine hydrochloride, L-cystine 2HCl, L-glutamine, L-histidine hydrochloride-H2O, L-isoleucine, L-leucine, L-lysine hydrochloride, L-methionine, L-phenylalanine, L-threonine, L-tryptophan, L-tyrosine disodium salt dihydrate, L-valine, magnesium sulfate ($MgSO_4$), niacinamide, potassium chloride (KCl), pyridoxal hydrochloride, Riboflavin, sodium bicarbonate ($NaHCO_3$), sodium chloride (NaCl), sodium phosphate monobasic (NaH_2PO_4-H_2O), thiamine hydrochloride, and i-inositol supplemented with 10% fetal bovine serum (FBS), nonessential amino acids (glycine, L-arginine, L-asparagine, L-aspartic acid, L-glutamic acid, L-proline, and L-serine, 20 μM each), and 1 mM sodium pyruvate (Thermo Fisher Scientific, Waltham, MA). Cells were passaged every 2-3 days and were used for experiments 16-24 hours after passage. For passage, cells were treated with 37 ℃ 0.25% trypsin for 1 min, resuspended in MEM, then plated with 2 mL of MEM per dish. Cells were maintained in a 37 ℃ / 5% CO_2 incubator. For electrophysiological recordings, the cells were collected from the culture dish using trypsinization. Briefly, cells were rinsed with PBS (NaCl, KCl, Na_2HPO_4, and KH_2PO_4), then treated with 37 ℃ 0.25% trypsin for 1 min before collection with MEM. Collected cells were kept in MEM at room temperature until used (within 4 hours).

2.2 NRVM Isolation

Neonatal rat experiments were approved by the Queen's University Animal Care Committee and performed in conformity with the Canadian Council on Animal Care. Sprague-Dawley rats of either sex were used for isolation of ventricular myocytes at 1 day of age. Neonatal rats were sacrificed by rapid decapitation with scissors followed by ventricle removal using scissors and

forceps. Ventricles were then washed twice with filtered PBS on ice and minced with scissors. The minced ventricles were washed twice with ice-cold PBS, and then incubated with 8.5 mL of PBS, 500 µL of collagenase (740 U), 500 µL of trypsin (370 U), and 500 µL of deoxyribonuclease (DNAse) (2880 U) at 37°C for 10 minutes to dissociate single ventricular myocytes. The supernatant was then extracted and placed in 20 mL of 20% FBS in Dulbecco's modified eagle medium/F12 (DF medium [formulation: thermofisher.com/ca/en/home/technical-resources/media-formulation.60.html]) supplemented with 3 mM $NaHCO_3$, 15 mM HEPES, and 50 mg/mL gentamycin). The enzymatic digestion and extraction were repeated six times. On the last three digestions, the minced ventricles were gently aspirated with a pipette to maximize the dissociation of cells. The cell mixture was then centrifuged at 95 g for 5 minutes. The supernatant was discarded. The viable cardiomyocytes were then extracted by Percoll density separation. Specifically, Percoll (GE Healthcare, Little Chalfont, UK) was diluted in appropriate amounts of Ads buffer (6.8 g of NaCl, 1.0 g of dextrose, 1.5 g of NaH_2PO_4, 0.4 g of KCl, 0.1 g of $MgSO_4$, and 4.76 g of HEPES in 1 L of double-distilled water) to create 10 mL of three separate densities: 1.050, 1.060, and 1.082 g/mL. Phenol red was added to the 1.060 g/mL solution to allow for distinction between the layers. First, 10 mL of the 1.050 g/mL solution was added to a new centrifuge tube. Next, 10 mL of a 1.060 g/mL solution was carefully added below using a pipette. Last, the cell pellet was resuspended in 10 mL of a 1.082 g/mL solution and carefully added below the 1.060 g/mL layer. The tube was then centrifuged at room temperature (22 ± 1°C) for 30 minutes at 483 g (with the brake disabled to avoid disrupting the gradient). The layer containing the cardiomyocytes (at the bottom of the red phase, between the 1.060 and 1.082 g/mL phases) was carefully removed with a micropipette, mixed in 45 mL of 10% FBS containing DF medium, and centrifuged for 5 minutes at 95 g. The pellet containing

cardiomyocytes was then resuspended in 20 mL of 10% FBS-containing DF medium and pre-plated on 100-mm plates. The plates were incubated at 37°C with 5% CO_2 for 45 minutes to allow fibroblasts to adhere to the bottom of the plate. The medium (containing cardiomyocytes) was then transferred to culture plates with glass coverslips and cultured overnight (for 16 hours) in 10% FBS in DF medium before electrophysiological recording.

2.3 Western Blot Analysis

After 16 hours of culture in media containing 10 µM of the respective drugs, hERG-HEK cells were collected with ice-cold PBS. Cells were lysed by sonication in ice-cold radioimmunoprecipitation assay lysis buffer supplemented with 1% phenylmethylsulfonyl fluoride and 2% protease inhibitor cocktail. A DC Protein Assay Kit (Bio-Rad, Hercules, CA) was used to determine the protein concentration of samples. Fifteen micrograms of protein sample was diluted to a volume of 40 µL with double-distilled water. The 40-µL sample was resuspended in 10 µL of 5× Laemmli loading buffer containing 5% β-mercaptoethanol to achieve a total volume of 50 µL, and boiled for 5 minutes. The 50-µL samples were separated on 8% SDS polyacrylamide electrophoresis gels and transferred overnight onto polyvinylidene difluoride membranes. The membranes were blocked for 1 hour using 5% non-fat milk. The blots were probed for 2 hours with the appropriate primary antibodies in 5% non-fat milk and then incubated with a 1:20000 dilution of the corresponding horseradish peroxidase (HRP)-conjugated secondary antibodies in 5% non-fat milk for an additional hour. Primary and secondary antibody incubations were followed by triple 10-minute washes in Tris-buffered saline/Tween 20 (0.1% Tween 20). The detection of actin was used as a loading control (CTL). Goat anti-hERG (C-20) primary antibody (Guo *et al.*, 2009), and mouse anti-goat HRP-conjugated secondary antibody (Skomedal *et al.*, 1999) were purchased from Santa Cruz

Biotechnology (Dallas, TX). Horse anti-mouse HRP-conjugated secondary antibody (Zhang *et al.*, 2008) was purchased from Cell Signaling Technology (Danvers, MA). The C-20 primary antibody was used in a 1:1000 dilution, the anti-actin primary antibody was used in a 1:2000 dilution, and the anti-mouse and anti-goat HRP-conjugated secondary antibodies were used in a 1:20,000 dilution. The blots were visualized with medical X-ray films (Fuji, Minato, Tokyo, Japan) using an enhanced chemiluminescence detection kit (GE Healthcare). Densitometry analyses of protein band intensities were performed using ImageJ in an unblinded manner. Boxes of equal sizes were positioned for each hERG and actin band as well as in a blank part of each lane to represent background, and the density was calculated. The background was then subtracted from corresponding band densities. Band sizes were identified using BLUeye Prestained Protein Ladder (GeneDireX, Inc., Keelung, Taiwan) loaded on each gel. For quantification, the band intensities of proteins of interest in each gel were first normalized to their respective actin (loading CTL) intensities and then expressed as values relative to the CTL.

2.4 Electrophysiological Recordings

The whole-cell voltage-clamp method was used to record various currents in HEK cells and isolated NRVMs. Whole-cell current-clamp was used to record APs from isolated NRVMs. Pipettes were pulled from thin-walled (0.19 mm) borosilicate glass (TW150-6; World Precision Instruments, Sarasota, CA) with a P-1000 micropipette puller (Sutter Instrument, Novato, CA) and polished with heat to a resistance of ~2.0 MΩ when filled with solution. An Axopatch 200B Amplifier, Digidata 1440A Digitizer, and Clampex version 10.7 software (Molecular Devices, San Jose, CA) were used for data acquisition and analysis. Current was sampled at 1 kHz and filtered at 5 kHz. Voltage was sampled at 100 kHz and filtered at 5 kHz. Recordings were carried out in simplified solutions. Although these solutions deviate from normal physiology, past

experience has shown that they produce reliable recordings. The pipette solution for recording from channels expressed in HEK cells, as well as I_K and APs from isolated NRVMs contained the following (in mM): 135 KCl, 5 EGTA, 5 MgATP, and 10 HEPES (pH 7.2 with KOH). The bath solution contained the following (in mM): 5 KCl, 135 NaCl, 2 $CaCl_2$, 1 $MgCl_2$, 10 glucose, and 10 HEPES (pH 7.4 with NaOH). The liquid junction potential (LJP) calculated with the Junction Potential tool in Clampex 10.7 was 4.3 mV and was not compensated. To create pH 6.4 bath solution, 6.0 M HCl was added drop-wise to normal bath solution (pH 7.4) until pH 6.4 was reached, measured by a digital pH meter. To create pH 8.4 bath solution, 1.0 M NaOH was added drop-wise to normal bath solution (pH 7.4) until pH 8.4 was reached, measured using a digital pH meter. To record I_{Na} and Ba^{2+}-mediated I_{Ca} ($I_{Ca\text{-}Ba}$), the pipette solution consisted of the following (in mM): 135 CsCl, 10 EGTA, 5 MgATP, and 10 HEPES (pH 7.2 with CsOH). For recording I_{Na}, the bath solution consisted of the following (in mM): 100 TEACl, 40 NaCl, 5 KCl, 1 $MgCl_2$, 10 glucose, and 10 HEPES (pH 7.4 with TEAOH). The calculated LJP was 6.4 mV and was not compensated. To record $I_{Ca\text{-}Ba}$, the bath solution consisted of the following (in mM): 140 TEACl, 5.4 $BaCl_2$, 1 $MgCl_2$, 10 glucose, and 10 HEPES (pH 7.4 with TEAOH). The calculated LJP was 3.0 mV and was not compensated. For acute concentration-response relationships, control current was first recorded in the absence of drug. Increasing concentrations of drug were then added, and the currents after steady state of block (within 1 min after drug application) were normalized to control. Normalized currents were plotted versus drug concentration to construct concentration-response relationships. Recordings were carried out at room temperature (22 ± 1°C).

2.5 Hypoxic Culture

For culture in hypoxic conditions, a C-Chamber incubator subchamber with a ProOx 110 oxygen controller (BioSpherix, Parish, NY) was used. 0.5% O_2 was maintained with a 95% N_2 / 5% CO_2 gas mixture, and temperature was maintained at 37 °C. Cells were passaged, then incubated for 6 hours in MEM buffered with sodium bicarbonate. Control cells were maintained in the same incubator, but outside of the hypoxic subchamber. Cells were collected for electrophysiological studies by trypsinization, re-suspended in hypoxic or normoxic media for control or hypoxia-treated cells respectively, and used within 1 hour.

2.6 Drugs and Reagents

Fentanyl citrate, norfentanyl hydrochloride, and naloxone hydrochloride were purchased from Toronto Research Chemicals (North York, ON, Canada). The powder form of fentanyl citrate was handled in a biological safety cabinet with proper protective equipment to minimize risk of exposure. Drugs were dissolved in double-distilled water and stored at −20°C. For patch-clamp experiments, the drugs were diluted in bath solution and used within 8 hours. For acute block, control solution was drained from the bath with a suction pump, and drug containing solution was immediately flowed in through a gravity-fed perfusion system. MEM, FBS, G418 (Geneticin), nonessential amino acids, and sodium pyruvate were purchased from Thermo Fisher Scientific (Waltham, MA). E-4031 (*N*-[4-[1-[2-(6-methylpyridin-2-yl)ethyl]piperidine-4-carbonyl]phenyl]methanesulfonamide) dihydrochloride was purchased from Tocris Bioscience (Bristol, UK), dissolved in double-distilled water stored at −20°C, and diluted in bath solution for patch-clamp experiments. Mouse anti-actin primary antibody (Kim *et al.*, 2007), ICA-105574 [ICA (3-nitro-*N*-(4-phenoxyphenyl) benzamide)], electrolytes, EGTA, HEPES, and glucose were

purchased from Sigma-Aldrich (St. Louis, MO). Collagenase Type 2, Trypsin, and DNase were purchased from Worthington Biochemical Corporation (Lakewood, NJ).

2.7 Statistical Analysis

Data in line graphs, scatter graphs, curves, and text are expressed as the mean ± S.D. For box plots, the middle line represents the median, the box encompasses the interquartile range, and whiskers represent the 5-95% range. For comparing multiple groups to control (CTL), a one-way analysis of variance (ANOVA) with Dunnett's post-hoc test was used to determine statistical significance. For comparing multiple groups to CTL and each other, a one-way ANOVA with Tukey's post-hoc test was used. For comparing one group to CTL, a two-tailed Student's *t* test were used. For normalized I-V and activation curves, a Wilcoxon matched pairs test was used to compare currents with fentanyl to CTL currents at each voltage. For normalized data with multiple groups, a Kruskal-Wallis test was used (post-hoc test was not required). For normalized data with multiple paired groups, a Friedman test with Dunn's post-hoc test was used. Statistical analysis was performed with GraphPad Prism (GraphPad Software, San Diego, CA). Where required, normality was tested in GraphPad Prism. Pulse currents recorded from hERG-HEK cells were analyzed as the maximal current during the last 50 milliseconds of the depolarizing step in Clampfit 10.4 (Molecular Devices, San Jose, CA). Tail currents recorded from hERG-HEK cells were analyzed as the maximal current during the first 500 milliseconds of the repolarizing step. Currents were fit using single or double exponential functions in Clamfit, with manual cursor placement to ensure an accurate fit. Half maximal inhibitory concentration (IC_{50}) values and Hill coefficients were determined by fitting data to the Hill equation ($y = \frac{A_1 - A_2}{1 + (\frac{x}{x_0})^p} + A_2$) in Microcal Origin 6.0 (OriginLab, Northampton, Massachusetts, USA). Voltages of half

maximal activation ($V_{1/2}$) values and slope factors were determined by fitting data to the Boltzmann function ($y = \frac{A_1 - A_2}{1 + e^{(x - x_O)/dx}} + A_2$) in Microcal Origin 6.0. For IC_{50} values, Hill coefficients, $V_{1/2}$ values, and slope factors, each cell was individually fitted and these values were summarized to determine the mean and S.D. A *P* value of 0.05 or less was considered to be statistically significant.

Chapter 3

Results

3.1 Fentanyl and Naloxone Block hERG Currents, but Norfentanyl Does Not

Whole-cell voltage-clamp was used to record I_{hERG} from hERG-HEK cells before and after drug application to the bath solution. I_{hERG} was elicited with the voltage protocol shown above the current traces at a start-to-start interval of 15 seconds. Because of the characteristic rapid inactivation properties (Spector *et al.*, 1996*b*), hERG channels activate and inactivate during the depolarizing step. Upon the repolarizing step, inactivated hERG channels rapidly recover to the open state and then slowly deactivate. This leads to the characteristic tail current, which represents maximal channel conductance, and was used to quantify the amplitude of I_{hERG}. Fentanyl blocked I_{hERG} in a concentration-dependent manner within seconds of drug application (Fig. 6A), and the blocked currents recovered completely within 1 minute upon washout. Although naloxone at concentrations much higher than clinically relevant doses (Blair *et al.*, 1989) also blocked I_{hERG}, norfentanyl did not block I_{hERG}. The amplitudes of I_{hERG} relative to CTL were plotted against corresponding fentanyl, norfentanyl, and naloxone concentrations, and fitted to the Hill equation when appropriate. Fentanyl blocked I_{hERG} with an IC_{50} of 0.9 ± 0.5 μM and a Hill coefficient of 0.9 ± 0.3. Naloxone blocked I_{hERG} with an IC_{50} of 74.3 ± 36.2 μM and a Hill coefficient of 0.9 ± 0.1. Norfentanyl did not affect I_{hERG} at concentrations up to 300 μM (Fig. 6B). The Hill coefficients of approximately 1 indicate that the binding of fentanyl to hERG channels is noncooperative.

3.2 Fentanyl-Mediated Decrease in I_{hERG} is not Reversed by Naloxone

Although HEK293 cells do not express the μ-opioid receptor (proteinatlas.org/ENSG00000112038-OPRM1/cell), to ensure that fentanyl-induced reduction of I_{hERG} cannot be prevented by naloxone, I applied fentanyl alone, and then fentanyl plus naloxone to the same hERG-HEK cells during patch-clamp recordings. Our results showed that 1 μM fentanyl reduced I_{hERG} by 50.0% ± 7.8% compared with CTL. When 1 μM fentanyl and 10 μM naloxone were applied together to the same cells, current was decreased by 58.1% ± 7.6% compared with CTL (Fig. 6C). Although addition of naloxone caused a slight further decrease in I_{hERG}, this change was not significant ($P > 0.05$, one-way ANOVA with Tukey's post-hoc test). Therefore, naloxone does not reverse the block of hERG channels by fentanyl. Further, when 10 μM naloxone was applied before fentanyl, it did not prevent I_{hERG} reduction (data not shown).

3.3 Fentanyl, Norfentanyl, and Naloxone Do Not Affect hERG Membrane Levels

To determine the chronic effects of fentanyl, norfentanyl, and naloxone on hERG channel expression, hERG-HEK cells were cultured overnight (for 16 hours) in media containing 10 μM of each compound. Whole-cell protein was then extracted and analyzed using Western blot analysis. Whole-cell hERG proteins display two bands (Zhou *et al.*, 1998). The lower (135-kDa) band represents the immature, core-glycosylated protein located in the ER. The upper (155-kDa) band represents the mature fully glycosylated protein located in the plasma membrane. Chronic treatment with 10 μM fentanyl, norfentanyl, or naloxone did not decrease hERG channel expression (Fig. 6D) or I_{hERG} after cells were removed from drug-containing solution (data not shown).

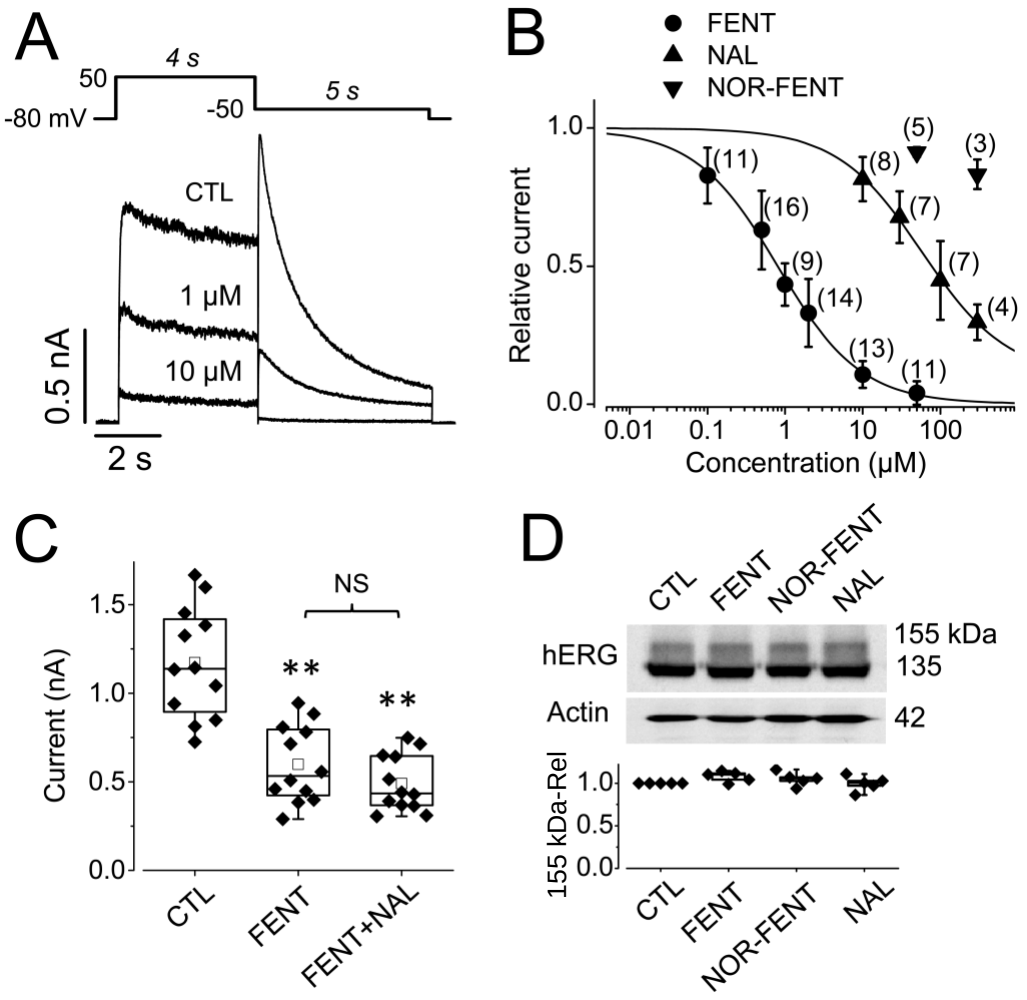

Figure 6. Fentanyl acutely blocks I_{hERG} but does not decrease hERG membrane protein expression.

(A) Representative hERG currents elicited using the voltage protocol above in control (CTL), and with 1 or 10 μM fentanyl. (B) Concentration-dependent effects of fentanyl (FENT), Naloxone (NAL), and Norfentanyl (NOR-FENT) on I_{hERG}. Currents after drug were normalized to current in CTL. The numbers above the data points indicate the number of cells examined from 4 independent experiments. Error bars represent S.D. I collected 30% of data. (C) Box plots of I_{hERG} recorded from control (CTL), in the presence of fentanyl (1 μM, FENT), or fentanyl (1 μM) plus naloxone (10 μM, FENT+NAL) (n=12, $^{**}P < 0.01$ *vs.* CTL, one-way ANOVA with Tukey's post-hoc test). I collected all data. (D) Western blot analysis of effects of 16-h treatment with fentanyl, norfentanyl, or naloxone (10 μM, respectively) on hERG expression. Actin is used as a loading control. The intensity of each hERG upper band was normalized to the actin and then to the control in each gel, and summarized (n=5, $P > 0.05$, Kruskal-Wallis test). Figure from Tschirhart *et al.* (2019).

3.4 Fentanyl-Mediated Block is Specific to hERG

To determine whether fentanyl blocks other K^+ channels, Jun Guo and Wentao Li studied the effects of fentanyl on hERG along with EAG, Kv1.5, KCNQ1 + KCNE1, Kv4.3, and Kir2.3 stably or transiently expressed in HEK cells. As shown in figure 7, acute application (within 5 seconds) of 10 μM fentanyl reduced I_{hERG} by 89.2% ± 7.1% ($P < 0.01$ compared with CTL, paired *t*-test) but did not reduce other channel currents studied ($P > 0.05$ compared with CTL, paired *t*-test).

3.5 Effects of Fentanyl on hERG Biophysical Properties

The effect of fentanyl on hERG voltage-dependence of activation was studied. Figure 8A shows families of hERG currents elicited with the voltage protocol above the current traces in the absence and presence of 1 μM fentanyl. The pulse currents measured at the end of the depolarization steps and the peak tail currents measured during the −50 mV repolarizing step, normalized to their respective maximal amplitude in CTL, were plotted versus activation (depolarization) voltages. The tail current-voltage relationships were fitted to the Boltzmann equation. In addition to block, fentanyl shifted the half-maximal activation voltage to negative voltages by 14.3 mV (−5.7 ± 2.8 mV in CTL; −20.0 ± 4.3 mV with fentanyl; $P < 0.01$, paired *t*-test). It also increased the slope factor from 6.6 ± 0.8 in CTL to 11.2 ± 2.1 ($P < 0.01$, paired *t*-test). Because of the changes in half-maximal activation voltage and slope factor, an interesting observation is that both pulse and tail I_{hERG} with fentanyl are slightly greater at depolarization voltages between −20 and −50 mV ($P < 0.01$, Wilcoxon matched pairs test) despite being reduced at 0 mV and above ($P < 0.01$, Wilcoxon matched pairs test) (Fig. 8A).

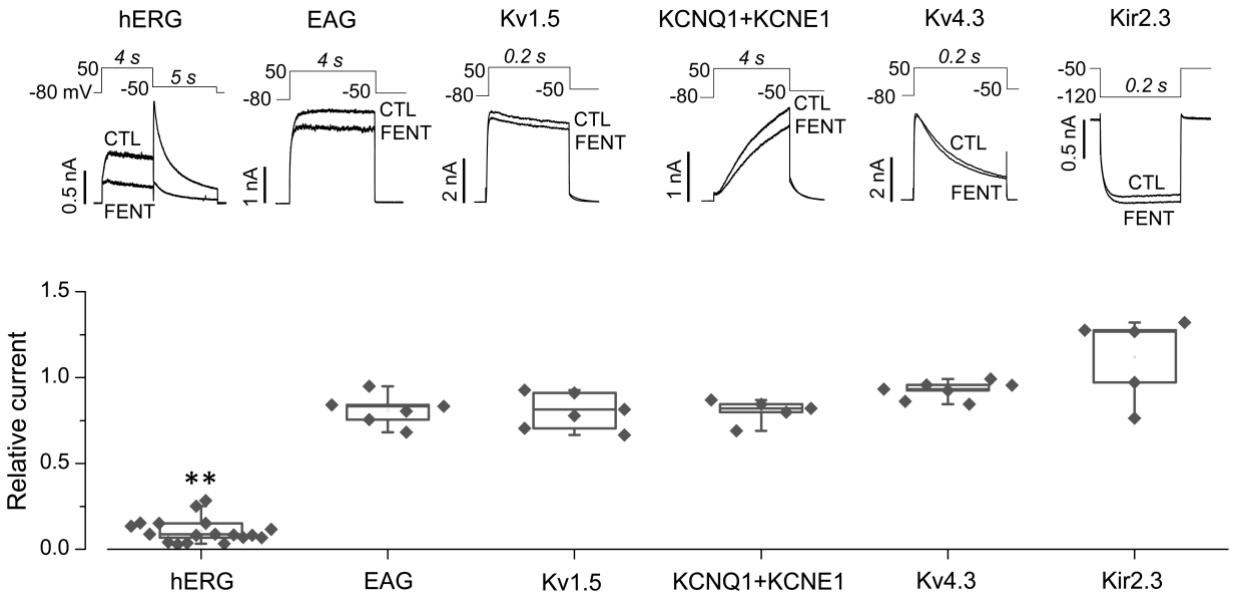

Figure 7. Fentanyl selectively blocks hERG channels.

Various currents elicited using the voltage protocol shown above in the absence (control, CTL) or presence of 10 µM of fentanyl (FENT) are shown (upper). Peak tail currents for hERG, pulse currents at the end of the depolarizing step for EAG, Kv1.5, and KCNQ+KCNE1, peak currents during the depolarizing step for Kv4.3, and inward currents at the end of the hyperpolarizing step for Kir2.3 were used for analyzing current amplitudes. Current amplitudes with fentanyl were normalized to their respective controls and summarized. To determine statistical significance, currents after fentanyl were compared to respective CTL current with paired *t*-tests for each channel. $^{**}P < 0.01$ *vs.* respective CTL, paired *t*-test. Data collected by Jun Guo and Wentao Li. Figure from Tschirhart *et al.* (2019).

We used a three-pulse voltage protocol to study the effects of fentanyl on hERG inactivation. hERG-HEK cells were depolarized to 60 mV for 500 milliseconds to activate and inactivate hERG channels. The cells were then repolarized to −100 mV for 5 milliseconds, allowing inactivated channels to recover to the open state with minimal deactivation (Zhou *et al.*, 1998). The third step to voltages between −30 and 130 mV in 10-mV increments was used to elicit hERG inactivation. The decay of hERG currents during the third step were fitted to single exponential functions to obtain the time constant of inactivation (τ_{inact}) values. Fentanyl decreased τ_{inact} at voltages of 0 mV and below ($P < 0.05$, paired *t*-test) (Fig. 8B).

To study the effects of fentanyl on hERG recovery from inactivation and deactivation, we depolarized cells to 60 mV for 1 second to activate and inactivate the channels. The cells were then stepped to voltages between 30 and −160 mV in 10-mV decrements to cause channel recovery from inactivation (the rising phase of currents) and deactivation (the decay phase of currents) (Fig. 8C). The rising phase of currents were fitted to single exponential functions to obtain the time constants of recovery from inactivation (τ_{recv}), which were plotted versus the repolarizing voltages. In the presence of fentanyl, there was an apparent shift in τ_{recv} values by approximately 25 mV in the negative direction (Fig. 8C). The decay phases of currents were fitted to double exponential functions to obtain the time constant of deactivation values, which were plotted versus the repolarizing voltages (Fig. 8D). For deactivation, only voltages between −90 and −160 mV were analyzed because deactivation was prominent and the current decay could be reliably fitted to determine the fast time constant of deactivation ($\tau_{f\text{-}deact}$) and the slow time constant of deactivation ($\tau_{s\text{-}deact}$). Fentanyl decreased $\tau_{f\text{-}deact}$ and $\tau_{s\text{-}deact}$ from −90 to −160 mV ($P < 0.05$ at each voltage, paired *t*-test).

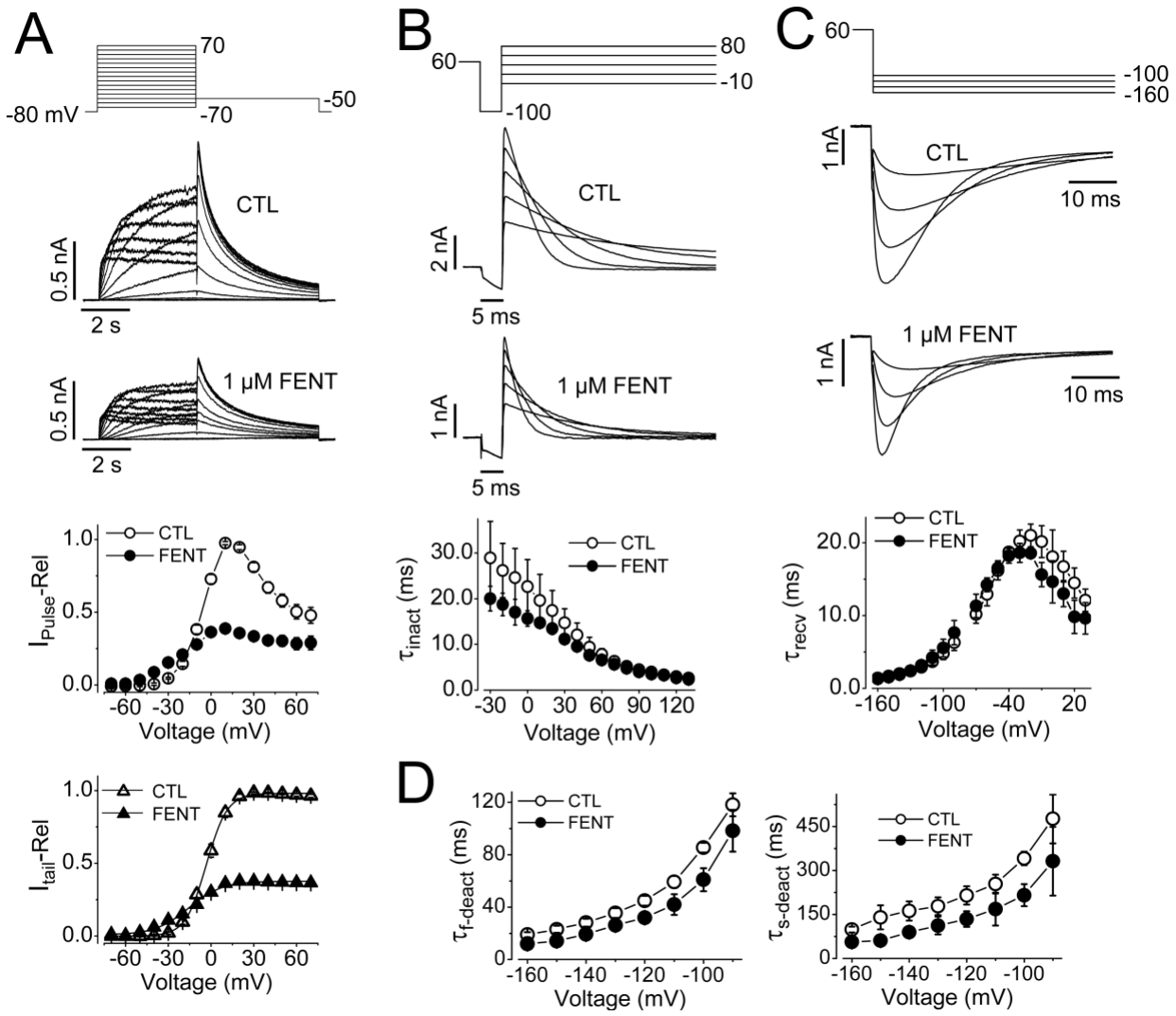

Figure 8. Effects of fentanyl on hERG biophysical properties.

(A) Voltage protocol, representative current traces, and summarized pulse and tail currents upon each depolarizing voltage in the absence (CTL, control) or presence of 1 μM fentanyl (FENT) are shown. The pulse current – voltage relationships were constructed by normalizing currents at the end of the depolarizing steps in the absence and presence of fentanyl to the maximal pulse current in control for each cell, and summarized against depolarizing voltages. The tail current – voltage relationships were constructed by normalizing the tail currents in the absence and presence of fentanyl to the maximal tail current in control for each cell, and plotted against depolarizing voltages (n=12). (B) Voltage protocol, representative currents (five traces, corresponding to the voltage protocol displayed, are shown for clarity), and τ_{inact} at corresponding voltages are shown (n=4). (C) Voltage protocol, representative currents (four traces corresponding to the voltage protocol are shown for clarity), and τ_{recv} plotted against test voltages are shown (n=5). (D) Fast ($\tau_{f\text{-}deact}$) and slow ($\tau_{s\text{-}deact}$) times constants of deactivating currents plotted against test voltages are shown (n=5). Error bars represent S.D. Figure from Tschirhart *et al.* (2019).

3.6 Fentanyl Blocks hERG in the Open State

To investigate whether fentanyl blocks hERG in the open state, we depolarized cells to 120 mV for 40 milliseconds to quickly activate the channels, followed by 4 seconds at 0 mV to maintain channel opening. The cells were finally repolarized to −50 mV for 500 milliseconds prior to returning to the holding potential of −80 mV. After recording CTL current, 2 μM fentanyl was immediately applied during the inter-pulse interval of 60 seconds when the cell was held at −80 mV. As shown in figure 9A, fentanyl-mediated block of hERG developed with time when channels were opened despite the drug being present for 1 minute prior to the channel opening. The time-dependent block was most obvious upon the first trace after fentanyl application (Fig. 9A, arrow a). Upon the second and subsequent depolarizing steps (Fig. 9A, arrow b), the initial current was largely blocked, but a slight development of block during the 0-mV step was still present. These data indicate that fentanyl preferentially blocks open channels, and a very small amount of unblock occurs during the inter-pulse interval when channels are closed at the holding potential of −80 mV as a steady state of block is present after the first trace.

Open-channel blockers can be trapped by channel closing upon repolarization (Mitcheson *et al.*, 2000*b*; Witchel *et al.*, 2004; Stork *et al.*, 2007). To investigate whether fentanyl can be trapped by hERG channel closing, we first achieved a steady state of channel block by recording hERG currents using the voltage protocol shown in the top of figure 9 for 5 minutes with 2 μM fentanyl present in the bath solution. We then completely washed out fentanyl (within 2 seconds) while cells were held at −80 mV for 60 seconds to maintain a closed channel state before applying the next depolarizing sweep to elicit hERG currents. As shown in figure 9B, when the channels were opened, the current gradually recovered (Fig. 9B, arrow a) to CTL level within the 4-second sweep. After the first trace of washout, the current remained at CTL levels (Fig. 9B,

arrow b). Thus, fentanyl is trapped by hERG channel closure and is released only upon channel opening.

3.7 Fentanyl Shares a Binding Site with Other Typical hERG Blocking Drugs

To characterize the binding site of fentanyl, Jun Guo examined its competition with E-4031, a well-studied hERG blocking drug (Sanguinetti & Jurkiewicz, 1990; Trudeau *et al.*, 1995; Spector *et al.*, 1996*a*). When I_{hERG} was recorded by repetitive pulsing to 50 mV for 4 seconds followed by −50 mV for 5 seconds at a start-to-start interval of 15 seconds, 10 μM fentanyl-mediated block was achieved after the first pulse during 20-minute recordings. Upon washout of fentanyl, I_{hERG} quickly recovered to 85.0% ± 18.9% of CTL (n = 4) (Fig. 10A, left). However, the recovery of I_{hERG} after 0.5 μM E-4031 block is minimal and slow to 10.1% ± 4.1% of CTL (n = 4) after a 10-minute washout (Fig. 10A, middle). To determine whether fentanyl and E-4031 compete for a common binding site on hERG, 10 μM fentanyl was applied to block the channel while an additional 0.5 μM E-4031 was applied in the same manner as when it was applied alone (Fig. 10A, right). Upon the washout of E-4031 and subsequently fentanyl, I_{hERG} recovered more than that from E-4031 block alone, to 43.2% ± 16.2% (n = 7, $P < 0.01$ vs. E-4031 alone, unpaired t-test). These data suggest that fentanyl may share binding sites with E-4031 to block hERG channels as E-4031 cannot access the binding site when fentanyl is present.

High-affinity binding of E-4031 and many other hERG blockers involves Tyr652 and Phe656 of the S6 transmembrane segment (Lees-Miller *et al.*, 2000; Mitcheson *et al.*, 2000*a*; Perry *et al.*, 2004; Guo *et al.*, 2006). Therefore, we examined fentanyl block in Y652A and F656T mutant channels. Y652A and F656T were resistant to block by 10 μM fentanyl ($P < 0.01$ vs. WT, one-way ANOVA with Dunnett's post-hoc test) (Fig. 10B), supporting the notion that fentanyl interacts with the typical hERG binding site involving residues Tyr652 and Phe656.

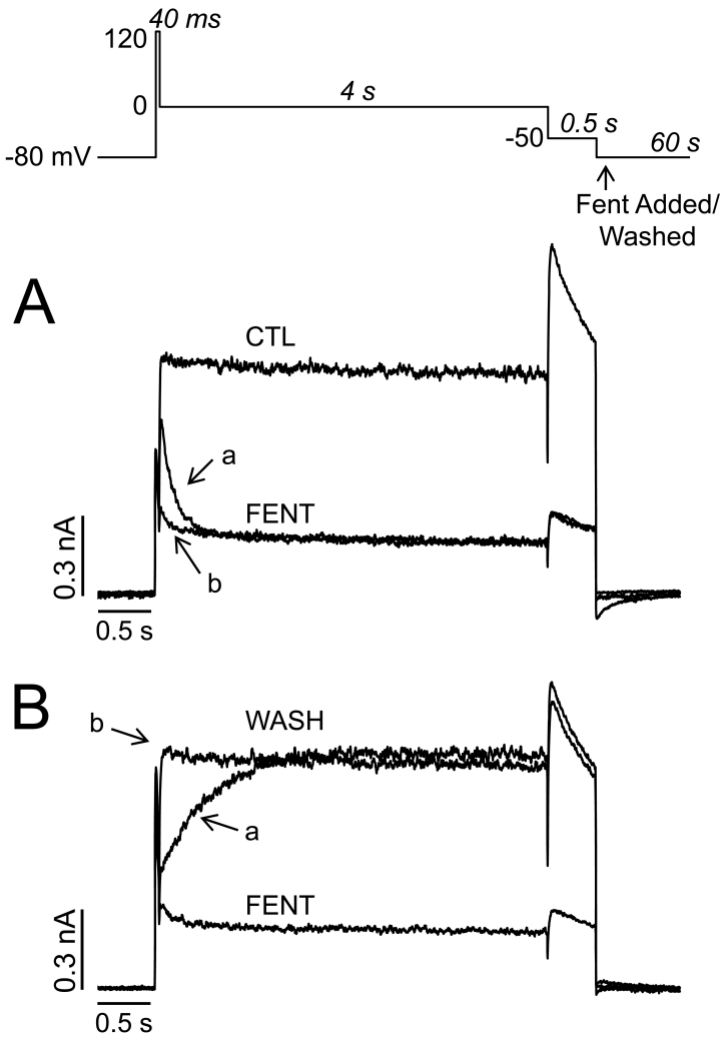

Figure 9. Fentanyl is an open channel blocker of hERG.

(A) hERG currents in control (CTL) and the first three traces in the presence of 2 µM fentanyl (FENT) recorded with the voltage protocol shown above. The first trace with fentanyl is indicated by arrow a, and subsequent traces by arrow b. The inter-pulse interval was 60 s, and fentanyl was immediately washed-in after the control current was recorded. (B) hERG current with fentanyl (FENT) and the first two traces after a complete washout of fentanyl (WASH). The first trace after fentanyl washout is indicated by arrow a, and subsequent trace by arrow b. The inter-pulse interval was 60 s, and fentanyl was immediately washed-out after the current with fentanyl was recorded. Figure from Tschirhart *et al.* (2019).

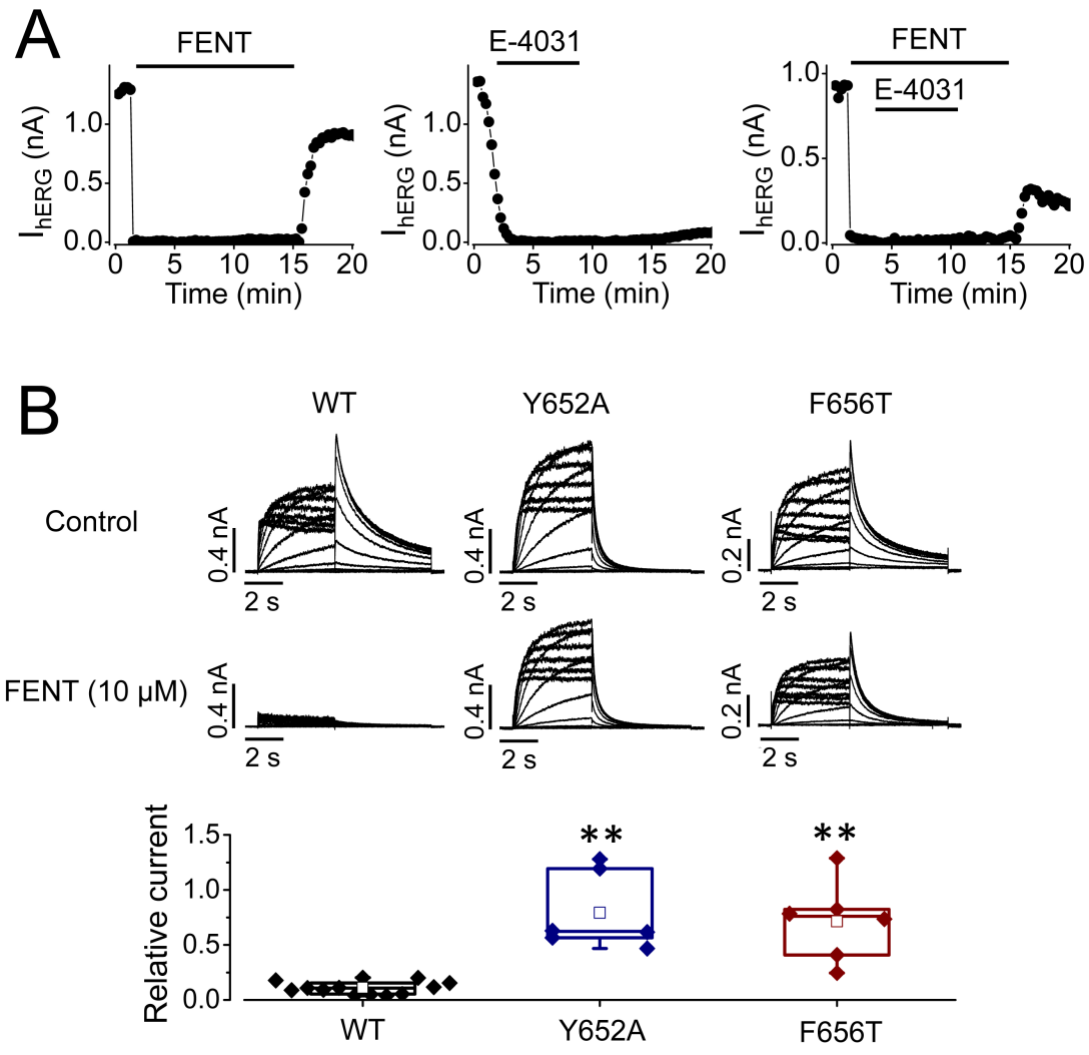

Figure 10. Fentanyl competes with E-4031 for binding to hERG channels.

(A) Blockade and washout of I_{hERG} (measured as peak tail current) by fentanyl, E-4031 and fentanyl plus E-4031. Left: I_{hERG} was rapidly blocked by 10 μM fentanyl, and largely recovered within 1 min upon fentanyl washout (n=4). Middle: I_{hERG} was blocked by 0.5 μM E-4031, and minimally recovered upon E-4031 washout (n=4). Right: Presence of fentanyl promoted I_{hERG} recovery upon E-4031 washout (n=7). Data obtained by Jun Guo. (B) The Y652A or F656T mutation decrease fentanyl-mediated block of I_{hERG}. While 10 μM fentanyl nearly abolished WT I_{hERG}, it affected neither Y652A nor F656T I_{hERG}. The voltage protocol is the same as figure 3A. Peak tail currents upon the −50 mV step after 50 mV depolarization were used for current amplitude analysis. The current with fentanyl was normalized to the control current in the same cell, and plotted in each group. $^{**}P < 0.01$ *vs.* WT, one-way ANOVA with Dunnett's post-hoc test). Figure from Tschirhart *et al.* (2019).

3.8 hERG Inactivation is not Required for Fentanyl Block

In addition to a common binding site, inactivation gating plays a critical role in high-affinity binding of various compounds to hERG channels (Wang *et al.*, 1997; Ficker *et al.*, 1998; Zhang *et al.*, 1999; Chen *et al.*, 2002). We examined whether fentanyl-mediated hERG block is also dependent on channel inactivation. To this end, we used three hERG inactivation mutants: S631A, S620T, and S620C. The Ser631 residue is located in the extracellular mouth of the pore (Schönherr & Heinemann, 1996). The S631A mutation causes a large positive shift in the voltage dependence of inactivation (Zou *et al.*, 1998) such that the resulting channels are essentially non-inactivating. Ser620 is located in the inner pore, and the mutation to Thr or Cys largely removes inactivation (Ficker *et al.*, 1998). In contrast to the notion that inactivation plays a critical role in drug-mediated hERG blockade, fentanyl blocked S631A and S620C mutant hERG currents more potently than WT (Fig. 11), whereas S620T decreased the potency of hERG block by fentanyl. The IC_{50} values were 0.9 ± 0.2 μM for WT (Hill coefficient, 1.1 ± 0.2), 0.5 ± 0.3 μM for S631A (Hill coefficient, 1.2 ± 0.2), 0.05 ± 0.07 μM for S620C (Hill coefficient, 0.6 ± 0.2), and 3.5 ± 1.4 μM for S620T (Hill coefficient, 1.1 ± 0.2). In particular, although both S620T and S620C removed hERG inactivation, they displayed very different sensitivities to fentanyl. Thus, unlike other hERG blockers (Wang *et al.*, 1997; Ficker *et al.*, 1998; Zhang *et al.*, 1999; Chen *et al.*, 2002), inactivation does not play an important role in fentanyl-mediated block of hERG channels.

3.9 Fentanyl Blocks hERG in a Voltage-Dependent Manner

We measured tail currents upon −50-mV repolarization after a 4-second 50-mV depolarizing step for WT hERG channels, but we measured pulse currents at the end of a 4-second 50-mV depolarization for inactivation-deficient mutant hERG channels to construct

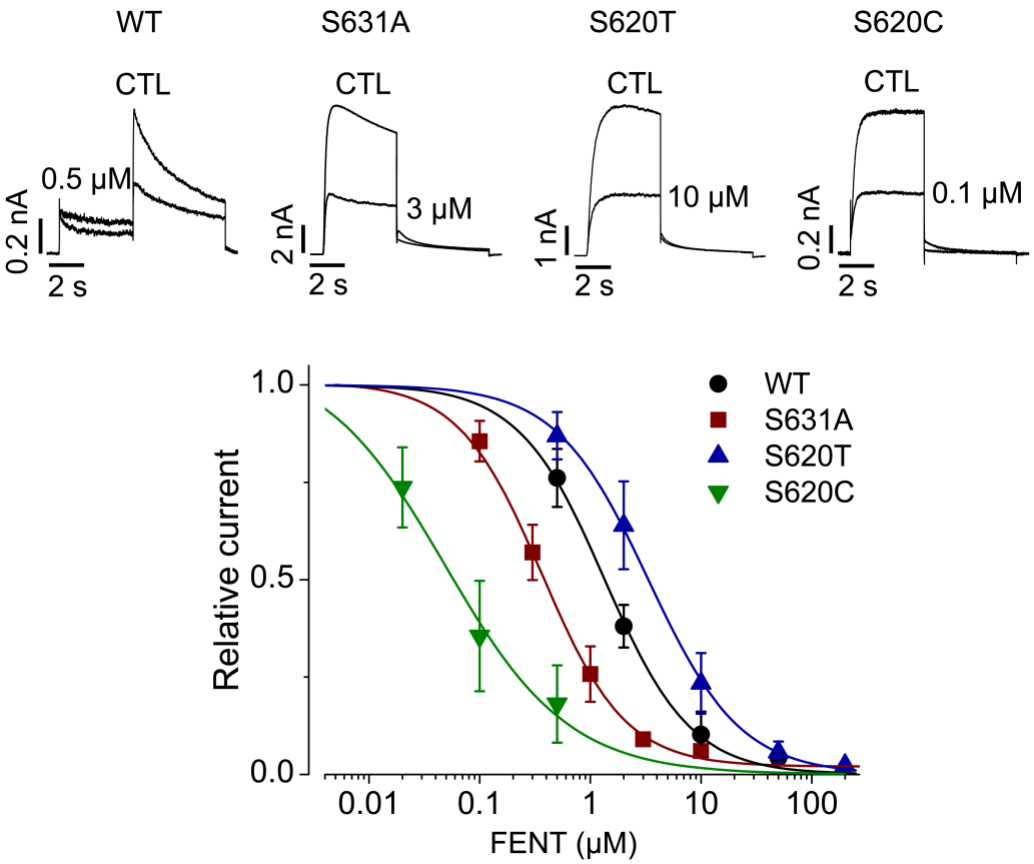

Figure 11. Inactivation does not play a role in fentanyl mediated block of hERG channels.

WT, S631A, S620T, or S620C hERG currents in the absence (control, CTL) or presence of fentanyl at various concentrations were elicited using the voltage protocol shown in figure 1A. Tail currents upon −50 mV after the 50 mV depolarizing pulse were used for analysis of WT channels, and current amplitudes at the end of the 50 mV depolarizing pulse were used for analysis of inactivation deficient mutant channels. Current amplitudes with fentanyl were normalized to control and plotted against drug concentrations. Data were fitted to the Hill equation to obtain IC_{50} values. Error bars represent S.D. WT, n=5; S631A, n=3-15; S620T, n=58; and S620C, n=4-8. Figure from Tschirhart *et al.* (2019).

concentration-response relationships. To investigate whether hERG block by fentanyl is voltage-dependent, we used inactivation-deficient channels to analyze fentanyl-mediated block at various voltages without interference from inactivation. Specifically, we used S631A and S620T mutant channels, as well as WT channels in the presence of 2 μM ICA, which removes inactivation (Gerlach *et al.*, 2010).

First, we recorded currents by depolarizing steps to voltages from −70 to 70 mV for 4 seconds in 10-mV increments followed by a repolarizing step to −50 mV for 5 seconds in the absence and presence of fentanyl (Fig. 12). For S631A, S620T, and WT with ICA, 3, 30, or 2 μM fentanyl was applied respectively to achieve a high degree of block while leaving some currents for analysis. The normalized pulse current-voltage and tail current-voltage relationships were constructed in the absence (CTL) and presence of fentanyl. Two observations are immediately obvious: First, fentanyl reduced the pulse currents to a greater extent than the tail current. Second, fentanyl decreased pulse current more at more positive voltages (Fig. 12).

The voltage-dependence of hERG channel block by fentanyl was examined further. From a holding potential of −80 mV, cells were depolarized to 50 mV for 4 seconds to activate channels. This was followed by test steps from 70 to −50 mV in 20-mV decrements for 5 seconds before returning to the holding potential (Fig. 13, top row). The current amplitudes after 100 milliseconds of test steps were plotted against the voltages to construct normalized current-voltage relationships. Although the currents increased with voltage in CTL, they were bell shaped in the presence of fentanyl (Fig. 13, middle row). When the ratio of current with fentanyl versus CTL was plotted against test voltage, it decreased linearly as voltage increased (Fig. 13, bottom row), demonstrating an increased block at higher voltages.

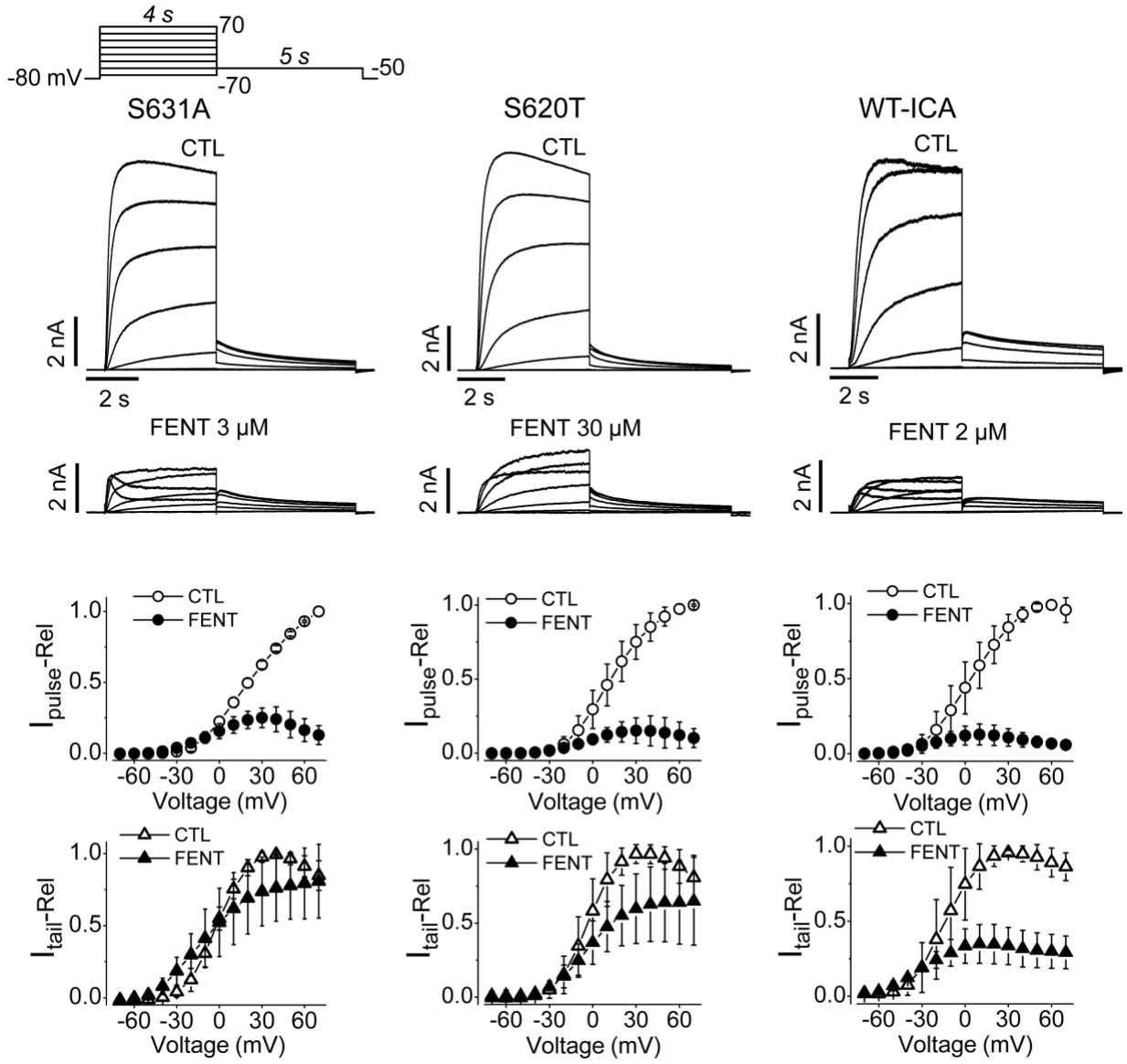

Figure 12. Fentanyl blocks pulse currents more than tail currents of inactivation-deficient hERG channels.

Representative currents recorded using the voltage protocol shown at the top are shown above the normalized pulse current- and tail current-voltage relationships. For normalization, pulse and tail currents in the absence and presence of fentanyl were normalized to their respective maximal currents in control for each cell, and plotted against the depolarizing voltages. While fentanyl largely reduced the pulse currents at positive voltages, it moderately reduced tail currents of S631A (n=5), S620T channels (n=8) or WT hERG with ICA-105574 (n=5). Error bars represent S.D. Figure from Tschirhart *et al.* (2019).

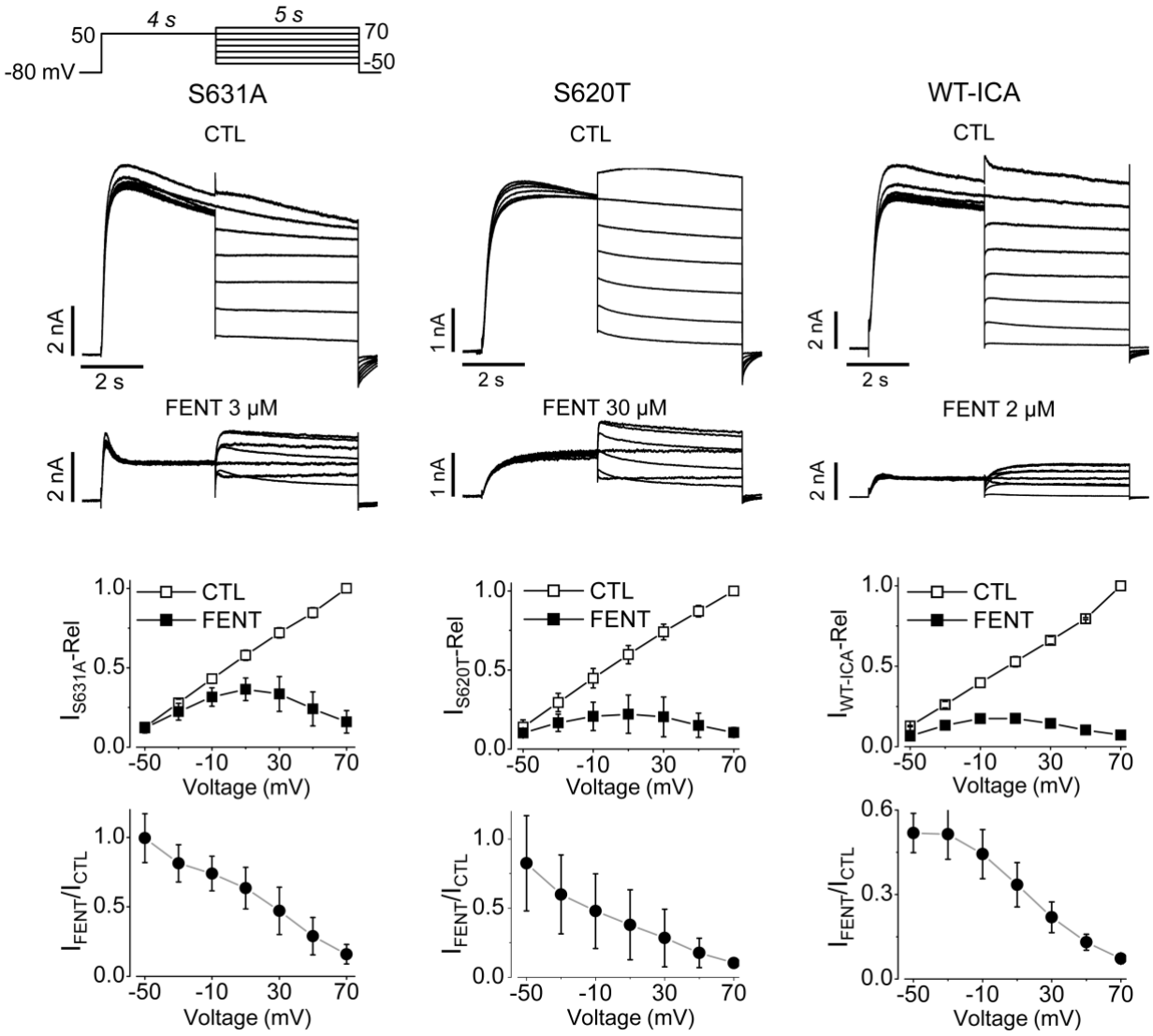

Figure 13. Voltage-dependence of fentanyl block of inactivation-deficient hERG channels.

S631A, S620T, and WT with ICA-105574 currents recorded using the voltage protocol shown above in the absence (control, CTL) or presence of 3, 30 or 2 µM fentanyl (FENT), respectively. The normalized current-voltage relationships in control (CTL) and with fentanyl (FENT) are shown in the middle. The currents measured after 100-ms of the test voltages between −50 and 70 mV in control and with fentanyl were normalized to the maximal currents in control for each cell, and plotted against the test voltages. Summarized ratios of currents with fentanyl versus currents in control plotted against test voltages are shown in the bottom. S631A, n=5; S620T, n=8; WT with ICA-105574, n=5. Error bars represent S.D. Figure from Tschirhart *et al.* (2019).

3.10 Fentanyl Blocks I_{hERG} with a Greater Potency Using an AP Voltage Protocol

When a ventricular AP voltage-clamp waveform is applied to hERG-HEK cells, hERG current activates rapidly, then increases as the membrane begins to repolarize, reaching a maximum at −20 to −30 mV (Zhou *et al.*, 1998). Given the voltage-dependence of fentanyl-mediated block of hERG channels, we were interested in examining how it affects hERG current during cardiac AP voltages. To this end, we used a human ventricular AP voltage-clamp waveform to elicit I_{hERG} and examined the concentration dependence of fentanyl block. Fentanyl blocked I_{hERG} with an IC_{50} of 0.3 ± 0.1 μM and a Hill coefficient of 0.9 ± 0.1 with this more physiologically relevant voltage protocol (Fig. 14).

3.11 Fentanyl Block of hERG is not Frequency-Dependent

To determine the IC_{50} for fentanyl block of hERG with the AP waveform protocol, we used a start-to-start interval of 2 seconds (a frequency of 0.5 Hz, Fig. 14). I was interested in determining whether the frequency of stimulation has an effect on degree of block. To this end, I applied the AP waveform protocol shown in figure 14 to hERG-HEK cells at the previously investigated frequency of 0.5 Hz and also at 1 Hz. After 9 seconds, I applied 2 μM of fentanyl. While it took slightly longer to reach steady state of block with a stimulation frequency of 0.5 Hz, the degree of block was not significantly different ($P > 0.05$, two-way ANOVA with Bonferroni post-hoc test comparing 0.5 Hz and 1 Hz at each time point) (Fig. 15). Twenty seconds after fentanyl application, drug solution was washed out with control solution. Stimulation frequency had no effect on the time course of recovery from block.

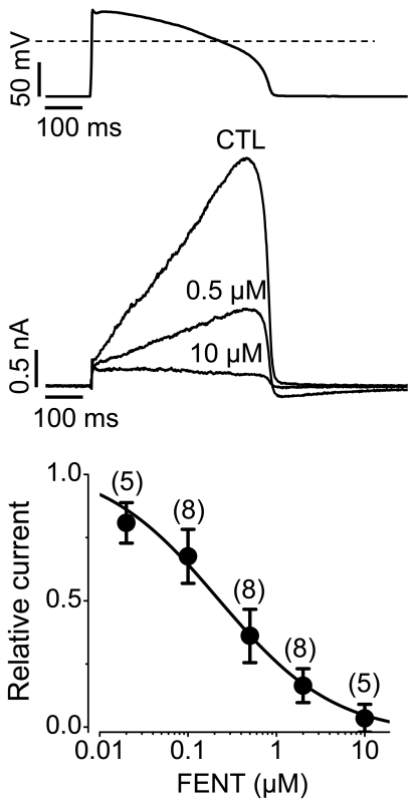

Figure 14. Effects of fentanyl on I_{hERG} elicited using a human ventricular action potential protocol.

The human ventricular action potential waveform (top) was applied to hERG-HEK cells to elicit I_{hERG}. The start-to-start interval was 2 seconds Representative currents in control (CTL), with 0.5 or 10 μM fentanyl are shown (middle). Peak hERG currents with various concentrations of fentanyl were normalized to the control current in each cell, and summarized against fentanyl concentrations. Data were fitted to the Hill equation. The numbers above the data points indicate the number of cells examined from 3 independent experiments. Error bars represent S.D. Figure from Tschirhart *et al.* (2019).

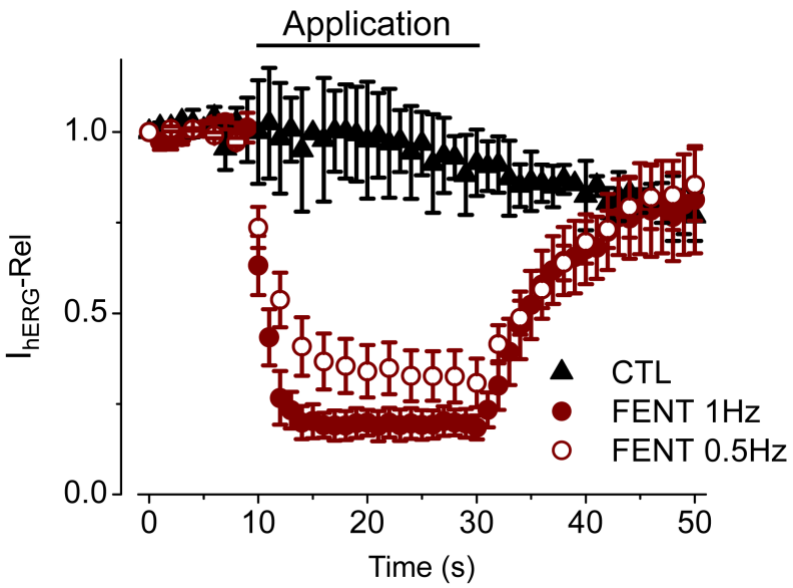

Figure 15. Block of hERG by fentanyl at different stimulation frequencies.

Cells were stimulated with the voltage protocol shown in figure 14 at a frequency of 0.5 Hz or 1 Hz. After 9 seconds of baseline recording, extracellular solution containing 2 μM fentanyl (FENT) was applied. As a control, extracellular solution not containing drug (CTL) was applied in the same manner. The peak hERG currents for each cell were normalized to the corresponding peak current during the first stimulation to facilitate comparisons, and summarized against time. For clarity, only data for 1 Hz stimulation of control are shown. CTL, n=3; FENT 1 Hz, n=5; FENT 0.5 Hz, n=6 from 1 independent experiment. Error bars represent S.D.

3.12 Fentanyl Decreases I_{Kr} and Prolongs APs in NRVMs

We examined the effects of fentanyl on the native I_{hERG} counterpart I_{Kr} as well as I_{Na} and I_{Ca} in isolated NRVMs. To determine the effects of fentanyl on I_{Kr}, we recorded I_K with a voltage protocol that first involves 1-second stepwise depolarizations from −70 to 70 mV in 10-mV increments, followed by a 1-second step at −50 mV before returning to a holding potential of −80 mV. As we previously demonstrated using this protocol, the tail current upon −50 mV repolarization primarily represents I_{Kr} (Guo *et al.*, 2007). Application of 0.5 μM fentanyl decreased tail current (Fig. 16A) ($P < 0.05$ at 10 mV and above vs. CTL, Friedman test with Dunn's post-hoc test at each voltage), with complete recovery upon washout (Fig. 16A) ($P > 0.05$ vs. CTL, Friedman test with Dunn's post-hoc test at each voltage). The tail current indeed represents I_{Kr} as it was essentially abolished by 1 μM of the selective I_{Kr} blocker E-4031 (Fig. 16A). On the other hand, fentanyl at a concentration of 10 μM did not affect I_{Na} or $I_{Ca\text{-}Ba}$ ($P > 0.05$, compared with CTL, Wilcoxon matched pairs test) (Fig. 16B&C).

Whole-cell current-clamp was used to record APs in isolated NRVMs stimulated with a 1 nA pulse. Fentanyl (0.5 μM) prolonged APD at 90% repolarization (APD_{90}) compared with CTL, and this effect was reversed upon washout (Fig. 16D). The mean APD_{90} was 298.3 ± 83.7 milliseconds for CTL, 404.4 ± 84.4 milliseconds with fentanyl ($P < 0.01$ vs. CTL, one-way ANOVA with Dunnett's post-hoc test), and 269.7 ± 71.7 milliseconds upon washout ($P > 0.05$ vs. CTL, one-way ANOVA with Dunnett's post-hoc test).

3.13 Chronic Hypoxia and Acute Fentanyl Decrease I_{hERG} in an Additive Manner

Chronic hypoxia has been shown to decrease I_{hERG} and I_{Kr} (Lamothe *et al.*, 2017). As fentanyl causes respiratory depression (McQueen, 1983), I was interested in investigating whether chronic hypoxia could potentiate hERG block by fentanyl. To address this, I cultured

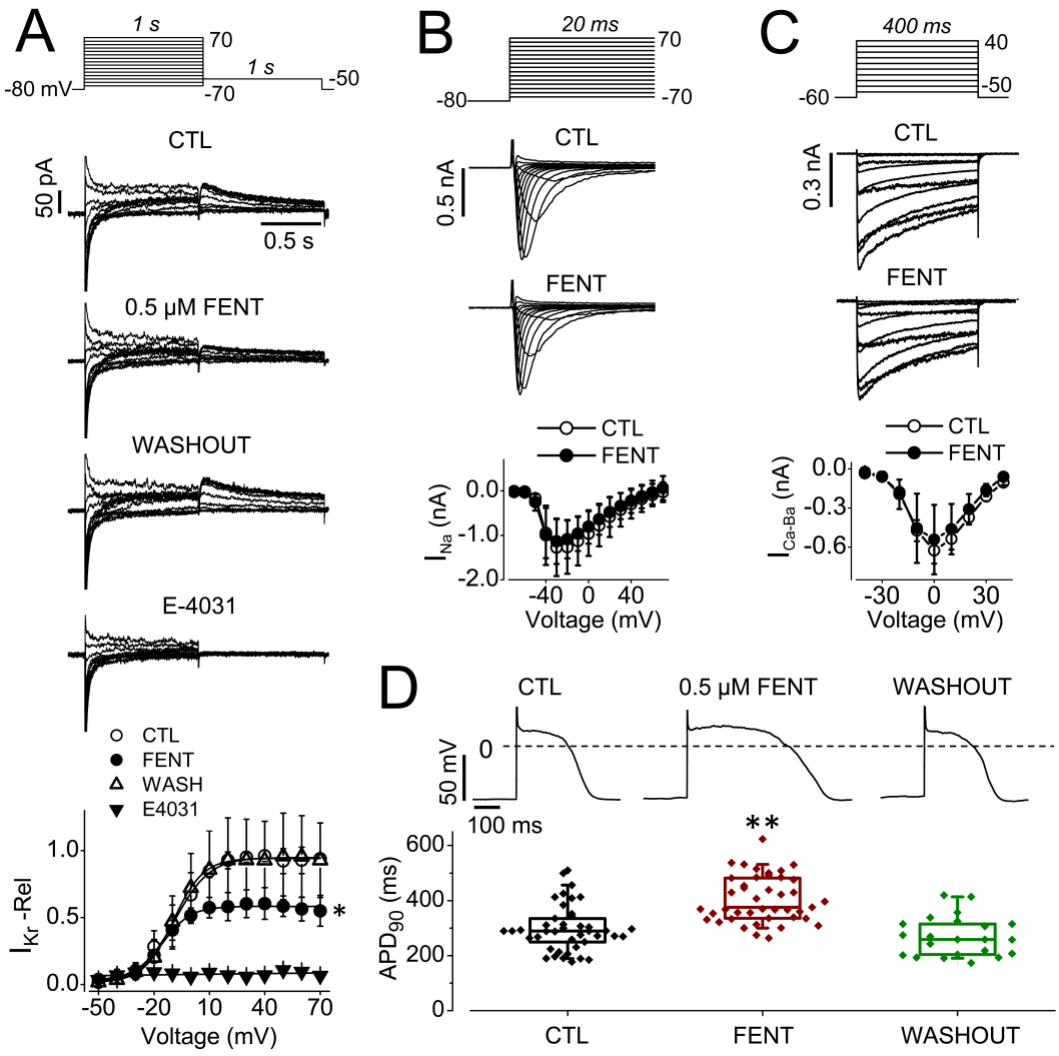

Figure 16. Fentanyl decreased I_{Kr} and prolonged action potentials in neonatal rat ventricular myocytes.

(A) Fentanyl-induced reduction of I_{Kr}. Representative I_K recorded from NRVMs in control, with 0.5 μM fentanyl, upon washout, and with 1 μM E-4031 are shown above summarized I_K-voltage relationships from 6 cells. E-4031 was used to demonstrate that tail current of I_K represents I_{Kr}, as it was selectively abolished. Tail currents at various voltages and conditions were normalized to the maximal tail current (following 70 mV depolarizing step) in control for each cell, and data from 6 cells were summarized. *$P < 0.05$ at 10 mV and above *vs.* CTL, Friedman test with Dunn's post-hoc test at each voltage. (B) Representative I_{Na} in control and with 10 μM fentanyl along with the summarized I_{Na}-voltage relationships (n=7). (C) Representative I_{Ca-Ba} in control and with 10 μM fentanyl along with I_{Ca-Ba}-voltage relationships (n=5). (D) Representative action potentials in control, with 0.5 μM fentanyl, and upon washout along with summarized APD_{90} (n=9 cells from 3 independent experiments, 42 action potentials for control and fentanyl, 22 action potentials for washout). **$P < 0.01$ *vs.* control, one way ANOVA with Dunnett's post-hoc test. Error bars represent S.D. Majority of data collected by Jun Guo and Wentao Li. I contributed 2 cells to panel A and D. Figure from Tschirhart *et al.* (2019).

hERG-HEK cells in 0.5% O_2 for 6 hours. As a control, cells from the same passages were cultured in normoxia, 21% O_2. As previously shown, 6 hours culture in 0.5% O_2 decreased average I_{hERG} by 52%. Currents recorded from normoxic cells were blocked 51 ± 9% by 1 μM fentanyl, while currents recorded from hypoxic cells were blocked 41 ± 12% ($P > 0.05$, unpaired *t*-test) (Fig. 17). Since there was no significant difference in the degree of block between normoxia and hypoxia groups, chronic hypoxia and fentanyl have an additive effect in reducing I_{hERG}, with average I_{hERG} after hypoxia and fentanyl being 79% of average control I_{hERG}.

3.14 N-terminal Deletion hERG Mutants are Blocked by Fentanyl with a Greater Potency

As there is evidence suggesting that native hERG channels are composed of 1a and 1b isoforms (Lees-Miller *et al.*, 1997; London *et al.*, 1997; Jones *et al.*, 2004; Phartiyal *et al.*, 2007), I was interested in examining if these channels are blocked by fentanyl with a different potency than the homotetrameric 1a channels studied thus far in this project. First, I examined fentanyl block of homotetrameric Δ2-354 hERG channels stably expressed in HEK cells (Δ2-354 hERG-HEK cells). These channels resemble hERG 1b, as the 1b isoform lacks the first 376 amino acids of 1a (Lees-Miller *et al.*, 1997; London *et al.*, 1997). I found that these channels were blocked with a greater potency than WT (hERG 1a) channels (Fig. 18). The IC_{50} values were 821 ± 130 nM for WT hERG (Hill coefficient, 1.0 ± 0.1), and 249 ± 67 nM for Δ2-354 hERG (Hill coefficient, 0.9 ± 0.2). Since fentanyl is trapped by channel closure (Fig. 9), I next wanted to determine if fast deactivation was responsible for the increased sensitivity of Δ2-354 hERG channels to fentanyl block. To this end, I examined Δ2-9 hERG channels transiently expressed in HEK cells. The Δ2-9 hERG mutant has also been shown to decrease deactivation time constants (Ng *et al.*, 2011), but a smaller deletion is less likely to alter channel structure and therefore allowed me to investigate the role of fast deactivation more directly. I found that Δ2-9 hERG

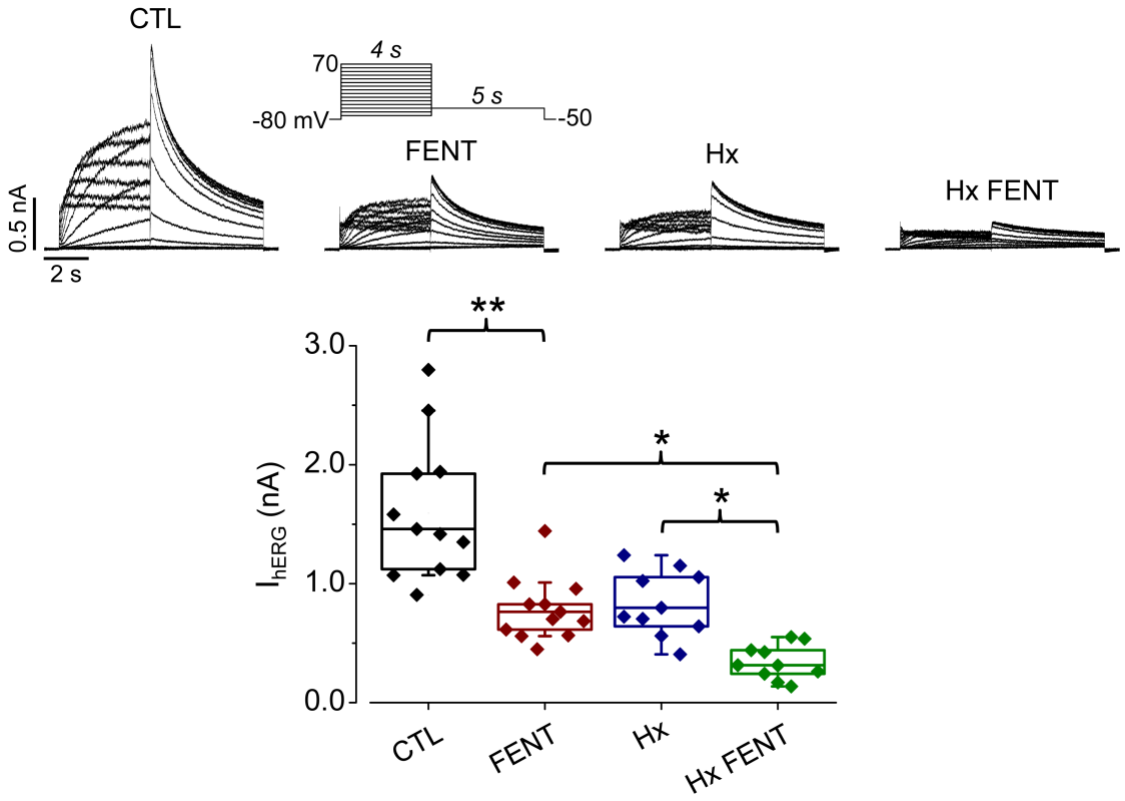

Figure 17. Combined effects of chronic hypoxia and acute fentanyl on I_{hERG}.

Cells were cultured in normoxia (CTL, 21% O_2) or hypoxia (Hx, 0.5% O_2) for 6 hours. For each cell, I_{hERG} was recorded in normal extracellular solution, before changing to extracellular solution containing 1 μM fentanyl (FENT). Representative current traces elicited with the voltage protocol are shown (top). The start-to-start interval was 15 seconds. Peak tail currents upon –50 mV repolarization after the 50 mV depolarizing step were used for analysis and are summarized in the box plot (bottom). CTL, n=12; FENT, n=12; Hx, n=10; Hx FENT, n=10 from 3 independent experiments. $^{**}P < 0.01$; $^{*}P < 0.05$, one-way ANOVA with Tukey's post-hoc test.

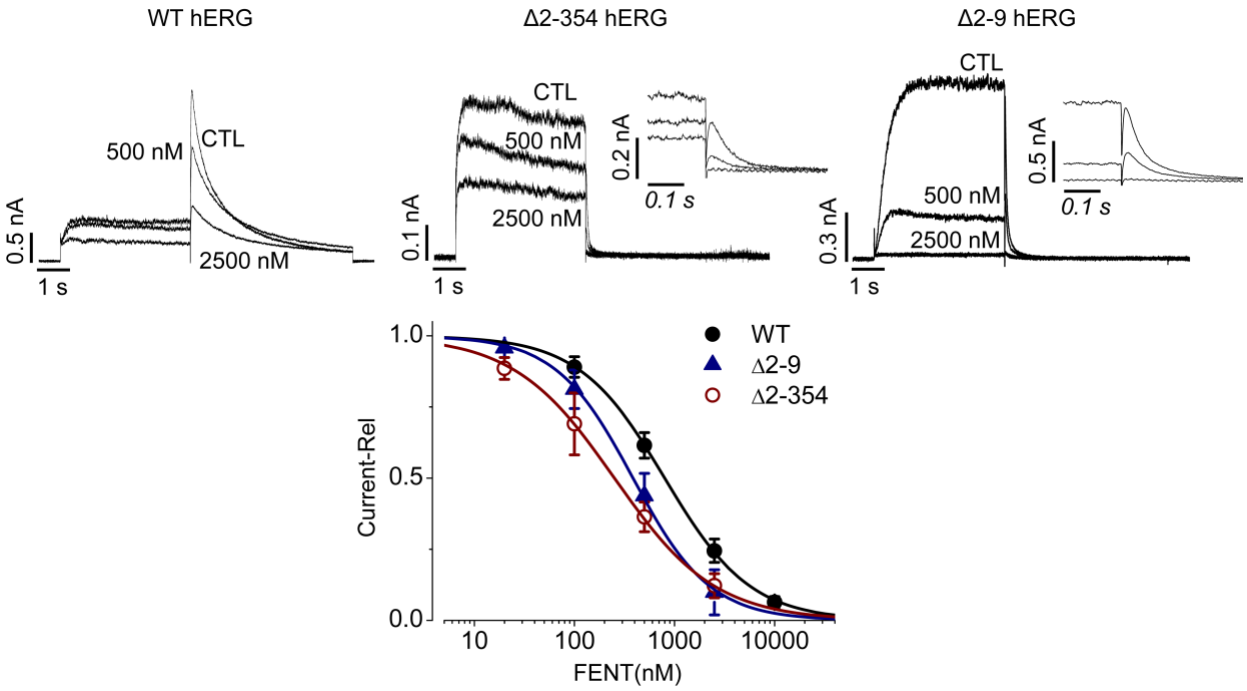

Figure 18. Block of N-terminal deletion hERG mutants by fentanyl.

Representative currents recorded from WT hERG-HEK cells, Δ2-354 hERG-HEK cells, and Δ2-9 hERG transiently expressed in HEK cells in control (CTL) solution and in the presence of 500 nM or 2500 nM of fentanyl (top). The voltage protocol was the same as figure 1A, and the start-to-start interval was 15 seconds. Tail currents upon –50 mV repolarization were used for analysis. The currents in the presence of each concentration of fentanyl were normalized to the current in control and plotted against fentanyl concentrations to construct the concentration-response relationship (bottom). Data were fit to the Hill equation to determine IC_{50} values. WT, n=10 from 4 independent experiments; Δ2-354 hERG, n=12 from 3 independent experiments and Δ2-9 hERG, n=5 from 2 independent experiments. Error bars represent S.D.

channels were also blocked with a greater potency than WT hERG (Fig. 18), with an IC_{50} of 403 ± 131 nM and a Hill coefficient of 1.1 ± 0.1. These data indicate that fast deactivation increases the block of hERG by fentanyl.

To establish the physiological significance of this increased block potency, we transiently co-transfected WT and Δ2-354 hERG into HEK cells in a 1:1 ratio, to resemble native hERG 1a/1b channels. Interestingly, these channels were also more sensitive to fentanyl than WT hERG (Fig. 19). The IC_{50} was 262 ± 54 nM and Hill coefficient was 1.0 ± 0.1. Therefore, the block of native channels by fentanyl may occur at lower concentrations than observed in cells expressing homotetrameric hERG 1a channels.

3.15 Fentanyl Block Potency is Dependent on Extracellular pH

The deactivation time constants of hERG channels are dependent on extracellular pH, with acidosis decreasing, and alkalosis increasing the time constants (Anumonwo *et al.*, 1999; Jiang *et al.*, 1999; Terai *et al.*, 2000). To further investigate the role of fast deactivation in determining the potency of hERG block by fentanyl, I examined fentanyl block at an extracellular pH of 6.4, where deactivation was faster. However, despite exhibiting fast deactivation, hERG channels were blocked with a lesser potency at pH 6.4 compared to pH 7.4 (Fig. 20A&B). The IC_{50} values were 2989 ± 589 nM for pH 6.4 (Hill coefficient, 1.0 ± 0.2), and 1069 ± 476 nM for pH 7.4 (Hill coefficient, 1.0 ± 0.2). I then performed a concentration-response experiment at pH 8.4. I found that despite slower deactivation, hERG channels were blocked with a greater potency at pH 8.4 compared to pH 7.4 (Fig. 20A&B), with an IC_{50} of 97 ± 38 nM and a Hill coefficient of 0.9 ± 0.04. To ensure that the enhanced sensitivity of I_{hERG} to fentanyl at pH 8.4 was due to channel blockade, I performed a washout experiment. First, at pH 7.4 I applied 3 μM fentanyl, which decreased I_{hERG} by 76 ± 6%. After washout (measured at

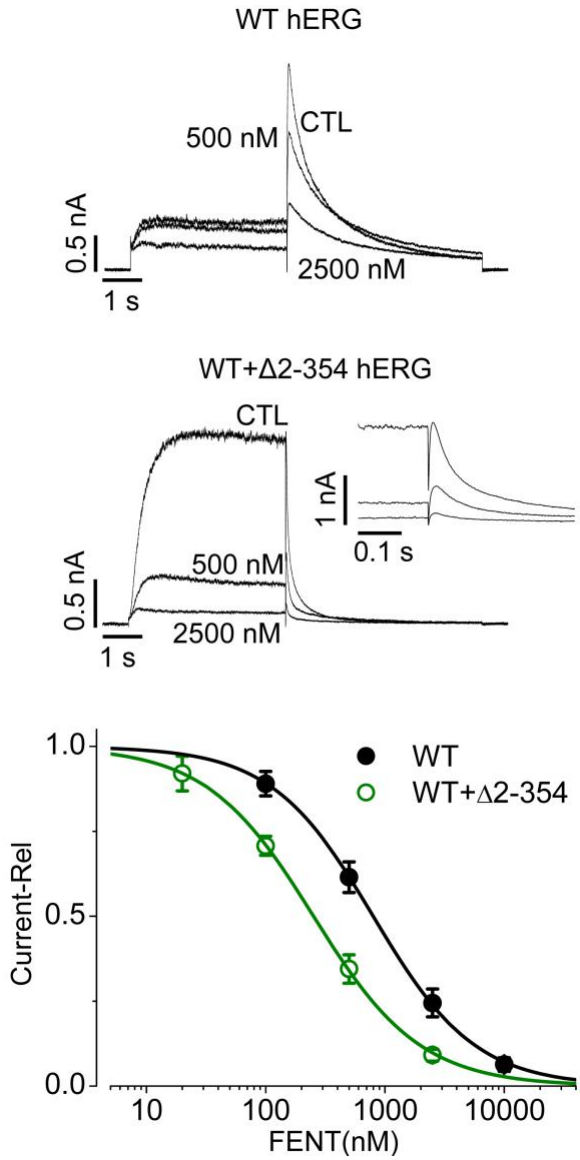

Figure 19. Block of co-expressed WT and Δ2-354 hERG channels by fentanyl.

Representative currents recorded from WT hERG-HEK cells (top), and WT with Δ2-354 hERG transiently co-expressed in HEK cells (WT+Δ2-354 hERG, middle) in control (CTL) solution and in the presence of 500 nM or 2500 nM of fentanyl. The voltage protocol was the same as figure 1A, and the start-to-start interval was 15 seconds. Tail currents upon –50 mV repolarization were used for analysis. The currents in the presence of each concentration of fentanyl were normalized to the current in control and plotted against fentanyl concentrations to construct the concentration-response relationship (bottom). The data for WT are the same as figure 18. Data were fit to the Hill equation to determine IC_{50} values. WT, n=10 from 4 independent experiments; WT+Δ2-354 hERG, n=8 from 2 independent experiments. Error bars represent S.D.

sweep 18), current recovered to 90 ± 3% of control (Fig. 20C). At pH 8.4, 3 μM decreased I_{hERG} by 93 ± 2%. However, this decrease was only partially reversed upon washout (measured at sweep 18), to 51 ± 17% compared to control ($P < 0.05$ compared to pH 7.4 washout, unpaired *t*-test) (Fig. 20C). Further, when the solution was then changed to pH 7.4, I_{hERG} recovered to control levels (data not shown). Therefore, hERG block by fentanyl is dependent on pH, with lesser block occurring at low values, and greater block occurring at high values.

3.16 Summary of Results

Our data showed that norfentanyl did not block I_{hERG} and that naloxone only blocked I_{hERG} at tens to hundreds micromolar concentrations. However, submicromolar concentrations of fentanyl blocked I_{hERG}, which could not be reversed by naloxone, indicating that reduction in current was through interaction between fentanyl and the channel rather than through opioid receptor signaling. Our data further revealed that fentanyl-mediated block of I_{hERG} was strongly voltage-dependent, but was independent of channel inactivation gating. Notably, block potency was increased when examined with a ventricular AP voltage protocol compared to a more traditional protocol. Fentanyl also blocked I_{Kr} and prolonged APs in NRVMs. In terms of clinical significance, I found that co-expressed hERG 1a/1b channels were blocked with markedly greater potency than hERG 1a channels. Additionally, hypoxia and alkalosis may potentiate the reduction of I_{Kr} by fentanyl block.

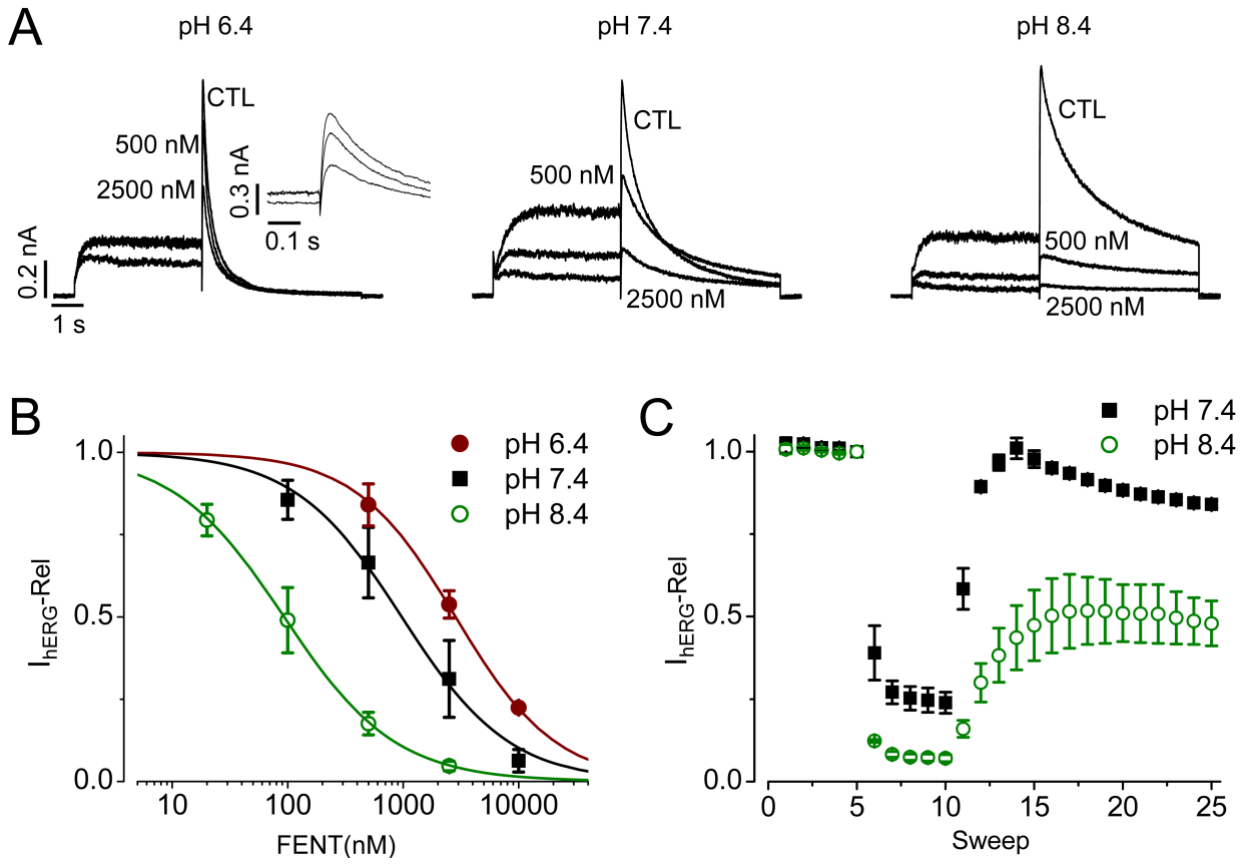

Figure 20. Effects of extracellular pH on hERG block by fentanyl.

(A) Representative currents recorded in extracellular solution with a pH of 6.4 (left), 7.4 (middle), or 8.4 (right) without drug (control, CTL) and in the presence of 500 nM or 2500 nM fentanyl. The voltage protocol was the same as figure 1A and the start-to-start interval was 15 seconds. (B) Tail currents upon –50 mV repolarization were used for analysis. The currents in the presence of each concentration of fentanyl were normalized to the current in control and plotted against fentanyl concentrations to construct the concentration-response relationship. pH 6.4, n= 3, pH 7.4, n=6; pH 8.4, n=4 from 2 independent experiments. (C) I_{hERG} was recorded with the same protocol as figure 1A with a start-to-start interval of 15 seconds in extracellular solution with a pH of 7.4 or 8.4. After 5 sweeps, solution of the corresponding pH containing 3 μM of fentanyl was added. After 5 additional sweeps, fentanyl was washed out with control solution of the corresponding pH. The data from each cell were normalized to the respective current on the fifth (last) baseline sweep. While there was a full recovery of I_{hERG} in pH 7.4 solution, there was only a partial recovery in pH 8.4 solution. pH 7.4, n=3; pH 8.4, n=3 from 1 independent experiment. Error bars represent S.D.

Chapter 4

Discussion

Fentanyl-associated death represents a serious issue in North America. Although fentanyl gives rise to respiratory depression (McQueen, 1983), it also prolongs the AP in isolated canine cardiac Purkinje fibers (Blair *et al.*, 1989). Katchman *et al.* (2002) described the effects of various opioid agonists including fentanyl, methadone, l-α-acetylmethadol, meperidine, codeine, morphine, and buprenorphine on I_{hERG} recorded from hERG-HEK cells. Although this study showed that fentanyl blocks I_{hERG} with an IC_{50} of 1.8 μM, and methadone blocks I_{hERG} in the closed and open/inactivated states, the mechanisms of fentanyl-hERG interaction and the effects of fentanyl on native I_{Kr} and APs in cardiomyocytes were not investigated.

The present project represents the first systemic investigation of the effects of fentanyl on I_{hERG} in hERG-HEK cells and I_{Kr} in NRVMs. My results revealed that, in contrast to many hERG blockers such as dofetilide, whose high-affinity binding requires channel inactivation (Ficker et al., 1998), fentanyl blocked hERG channels in the open state (Fig. 9), but inactivation gating did not play a role in the fentanyl-hERG interaction (Fig. 11). I also demonstrated that fentanyl decreased I_{Kr} and prolonged APD_{90} in NRVMs (Fig. 16).

Regarding the molecular mechanisms that underlie fentanyl-mediated hERG block, my project revealed that whereas fentanyl shares some properties with other hERG blockers, it possesses several novel properties. Previous mutagenesis and electrophysiological assays have shown that residues Thr623 and Val625 of the pore helix, and Gly648, Tyr652, and Phe656 of the S6 transmembrane segment are crucial for high-affinity binding of various compounds (Mitcheson *et al.*, 2000*a*). Although I did not examine Thr623, Val625, or Gly648 mutations, I did show that Y652A and F656T mutant hERG channels are resistant to block by fentanyl (Fig.

10B). Furthermore, Jun Guo found that fentanyl competed with E-4031 for binding to hERG (Fig. 10A), suggesting that fentanyl occupies the common drug-binding site within the internal pore-mouth of the hERG channel. I propose that fentanyl enters the binding site of the channel and interacts with residues that line hydrophobic pockets (Wang & MacKinnon, 2017). Non-covalent π-stacking interactions occur between two aromatic rings, where the positive potential of one ring aligns with the negative potential of the other, creating a strong association. The aromatic side chain of fentanyl may form π-stacking interactions with residues in the hydrophobic pockets including Tyr652 and Phe656, leading to blockade.

In support of this theory, norfentanyl, the main metabolite of fentanyl produced when the phenyl-containing side chain is removed through N-dealkylation by liver enzymes (Goromaru *et al.*, 1984; Tateishi *et al.*, 1996), does not block I_{hERG} (Fig. 6B). This is in contrast to O-demethylation of astemizole, which generates the principle metabolite desmethylastemizole that blocks hERG channels with a similar potency (Zhou *et al.*, 1999). However, N-dealkylation of astemizole, which removes a phenyl-containing side chain to create norastemizole (a secondary metabolite), decreases block potency (Zhou *et al.*, 1999). This indicates that side chains containing phenyl groups are important for hERG block by drugs like fentanyl and astemizole. Since fentanyl is primarily metabolized to norfentanyl, the difference in hERG blocking properties is of clinical significance. First, drugs or conditions that decrease liver enzyme activity would increase fentanyl concentration, increasing the risk of hERG block. Second, naloxone does not reverse the decrease in I_{hERG} by fentanyl (Fig. 6C). Increasing liver enzyme activity is a promising therapeutic intervention for fentanyl-induced hERG toxicity, where arrhythmias and sudden death represent a concern.

Inactivation plays a critical role in high-affinity hERG binding by many compounds such as dofetilide, verapamil, E-4031, and cisapride (Ficker *et al.*, 1998; Zhang *et al.*, 1999; Chen *et al.*, 2002). Given that fentanyl appears to block hERG through targeting a typical binding site, it is interesting that unlike many compounds, inactivation does not play a role in hERG block by fentanyl (Fig. 11). The reason for this discrepancy is unknown but is likely related to the distinct tertiary structure of fentanyl, for which inactivation-induced conformational change of hERG is not required for high-affinity binding. In this regard, our lab previously demonstrated that inactivation does not play a role in cocaine block of hERG channels (Guo *et al.*, 2006).

My results showed that whereas S631A and S620C were blocked by fentanyl with a greater potency than WT channels, S620T displayed a reduced sensitivity (Fig. 11). S620T is consistently more resistant to block than other inactivation-deficient mutants (Ficker *et al.*, 1998; Zhang *et al.*, 1999; Guo *et al.*, 2006). Since Ser620 is within the inner pore of hERG (Ficker *et al.*, 1998; Chen *et al.*, 2002), it may be involved in drug interaction with the channel. Although the Cys molecule, similar in size to the Ser residue in WT, conserves the high-affinity binding site, the larger Thr residue may disrupt it. In support of this theory, despite disrupting inactivation to the same extent, hERG channels with four S620T subunits are more resistant to cisapride, dofetilide, and MK-499 block than channels with one S620T subunit and three WT subunits (Wu *et al.*, 2015). Thus, I believe that fentanyl block is not associated with inactivation. However, channel opening is a prerequisite for fentanyl to block hERG channels as block does not develop until the channel is open (Fig. 9A). Once open, the block clearly develops in the first trace after fentanyl application and smaller currents with decay were observed in subsequent traces. This small decay is consistent with fentanyl being trapped with minimal unbinding when

hERG is held in the closed state. Even after completely removing fentanyl from the bath solution, I_{hERG} does not recover until the channels are opened (Fig. 9B).

Another interesting finding is the voltage-dependence of hERG block by fentanyl. Using hERG channels with inactivation removed by mutations or drug, my results demonstrated a nearly linear voltage-dependence of fentanyl block between −50 and 70 mV, with greater block at more positive voltages (Fig. 13). Like most hERG blockers such as verapamil (Zhang *et al.*, 1999), I propose that fentanyl enters the binding site within the pore from the internal side of the membrane. Fentanyl has a pK_a of 8.12 at 37 ºC, thus it is mostly positively charged at physiologic pH (Thurlkill *et al.*, 2005). Therefore, positive voltages may repel the positively charged fentanyl molecules deeper into the internal pore mouth. Upon discovering that fentanyl blocks hERG in a voltage-dependent manner, I investigated fentanyl block with a cardiac AP waveform voltage protocol. Interestingly, whereas the IC_{50} for fentanyl block determined by measuring the tail current at −50 mV after channel activation at 50 mV was 0.9 μM (Fig. 6A&B), it was 0.3 μM when analyzed using the more physiologically relevant AP voltage protocol (Fig. 14). This difference in potency is primarily due to voltage-dependent block, as peak hERG current during the AP protocol occurs at voltages more positive than −50 mV. This finding is clinically important because the hERG blocking effects of fentanyl are 6-fold more potent than originally described by Katchman *et al.* (2002).

While investigating the block of I_{hERG} elicited by the AP waveform voltage protocol, I was interested in determining whether stimulation frequency affected the degree of fentanyl block. Some hERG blocking drugs, such as verapamil (Zhang *et al.*, 1999) and cisapride (Walker *et al.*, 1999) block hERG to a greater extent at faster stimulation frequencies. Such frequency dependence is clinically significant as I_{Kr} reduction would become greater at faster heart rates.

However, I found that fentanyl did not block hERG to a greater degree at a stimulation frequency of 1 Hz compared to 0.5 Hz (Fig. 15). Due to the length of the AP stimulus waveform, higher frequencies could not be studied. Nonetheless, this data indicates that the frequency of stimulation, or heart rate, does not affect hERG block by fentanyl. A possible explanation for this observation is the fast binding of fentanyl to hERG channels, and the trapping by channel closure (Fig. 9). As binding occurs quickly, channels do not need to be open for a long period for block to occur, and therefore the number of stimulations required to develop steady state block is low. Additionally, since fentanyl is trapped in the channel pore when channels are closed, the amount of block is not affected by the length of time between stimulations.

I also found that hERG N-terminal deletion mutant channels were blocked by fentanyl with a greater potency (Fig. 18). In these experiments the IC_{50} for WT channels was 821 nM, while channels with the majority of the N-terminus deleted (Δ2-354) demonstrated an IC_{50} of 249 nM. As Δ2-354 channels exhibit fast deactivation, I proposed that fast deactivation traps more fentanyl in the pore, increasing block potency. To examine this, I investigated fentanyl block of Δ2-9 hERG channels, which also exhibit fast deactivation, but the shorter deletion is less likely to impact channel structure. The IC_{50} for Δ2-9 hERG channels was 403 nM, consistent with my theory that fast deactivation underlies increased fentanyl potency because the deactivation time constants of Δ2-9 hERG are intermediate to those of WT and Δ2-354 hERG (Ng *et al.,* 2011). Of clinical significance, when WT and Δ2-354 hERG were co-expressed, these channels were blocked with an IC_{50} of 262 nM (Fig. 19). Co-expressing WT and Δ2-354 hERG was intended to resemble heterotetrameric hERG 1a/1b channels present *in vivo*. Interestingly, the IC_{50} for these channels was similar to Δ2-354 hERG expressed alone. These data are inconsistent with the notion that fast deactivation is responsible for enhanced fentanyl potency,

as co-expressed WT and Δ2-354 hERG have deactivation time constants that are intermediate to WT and Δ2-354 hERG expressed alone. Therefore, the full mechanism underlying enhanced fentanyl block of co-expressed WT and Δ2-354 hERG requires further investigation.

While investigating the role of fast deactivation in determining fentanyl block potency, I made the serendipitous discovery that fentanyl block of hERG is pH-dependent. I intended to use modification of extracellular pH as a tool to alter the deactivation speed of hERG channels (Anumonwo *et al.*, 1999; Jiang *et al.*, 1999; Terai *et al.*, 2000) without deleting part of the N-terminus. However, despite exhibiting the expected fast deactivation, hERG channels were blocked with a reduced potency at extracellular pH 6.4 compared to pH 7.4 (Fig. 20A&B). Further, hERG channels were blocked with an increased potency at extracellular pH 8.4 compared to pH 7.4 whilst exhibiting the expected slow deactivation (Fig. 20A&B). There are several potential explanations for this phenomenon, though they are not mutually exclusive. First, high pH may increase the membrane permeability of fentanyl. As fentanyl is a weak base with a pK_a of 8.12 at 37 ^oC (Thurlkill *et al.*, 2005), it is predominately positively charged at a pH of 7.4. At a pH of 8.4, most of the molecule is in the neutral form, so it likely crosses the cell membrane more easily. As our data suggest that fentanyl blocks hERG through an intracellular mechanism (Fig. 13), enhanced membrane permeability would be expected to increase block potency. However, despite being positively charged fentanyl appears to be fairly efficient at crossing biological membranes. At physiological pH fentanyl readily crosses the blood-brain barrier to act at receptors in the central nervous system (Hug & Murphy, 1979). Furthermore, a study of buccal fentanyl absorption in canines found that a 10-fold increase in unionized fentanyl concentration only increased the permeability coefficient by 5-fold, suggesting that the ionization state of fentanyl may not directly determine membrane permeability (Streisand *et al.*, 1995).

Another possible explanation for the extracellular pH-dependence of fentanyl block is that the neutral form of fentanyl has a higher affinity for the hERG channel than the positively charged form. This possibility has merit, as our findings suggest that fentanyl interacts with hydrophobic residues lining the pore of the channel (Fig. 10). Therefore, an uncharged, hydrophobic fentanyl molecule would interact more strongly with these residues than one that is positively charged. Additionally, we showed that positive depolarizations dramatically increase degree of block (Fig. 13), which suggests that the charged form of fentanyl may not have a high affinity for hERG channels. This theory is supported by the fact that when fentanyl is applied at pH 8.4, the reduction in I_{hERG} is only partially reversed upon washout of the drug (Fig. 20C). This result suggests that neutral fentanyl molecules form strong interactions with the hydrophobic residues in the pore of the hERG channel, and do not dissociate readily. In fact, after blocking channels at pH 8.4, washing out the drug with pH 7.4 solution restores current to control levels (data not shown). It is likely that returning the extracellular solution to normal pH adds positive charge to most fentanyl molecules, weakening interactions with hERG channels. A potential flaw in this theory is the pipette solution remained at pH 7.2 for these experiments; therefore, once inside the cell the majority of fentanyl would be positively charged. However, the pore of hERG is open to the extracellular side of the membrane (Wang & MacKinnon, 2017). Thus, it is possible that the high pH of the extracellular solution is conferred to the pore of the channel. Once fentanyl molecules are in the pore, they may become unionized and bind to aromatic residues with the proposed high affinity. This scenario is supported by evidence suggesting that the pore of hERG can become blocked by protons at pH values lower than those studied here (Bett & Rasmusson, 2003; Van Slyke *et al.*, 2012), indicating that extracellular pH can affect the environment within the pore. The alteration of pH within the channel pore presents

the final possibility. Such a change in pH may alter channel structure and ionization state of residues, which could create a higher affinity binding site for fentanyl. It remains possible that several of these explanations are true and together account for the enhanced potency of fentanyl block at high pH.

We have shown that fentanyl blocked I_{hERG} with an IC_{50} of 0.3 μM (Fig. 14), and it prolonged the cardiac AP at a concentration of 0.5 μM (Fig. 16D). A retrospective study (Martin *et al.*, 2006) based on 112 fentanyl-related deaths reported that the mean postmortem blood concentrations in deaths attributed solely to fentanyl was 25 μg/l (74.3 nM), with a range of 3 μg/l (8.9 nM) to 383 μg/l (1.14 μM). Although the IC_{50} for fentanyl to block hERG is higher than the mean postmortem blood level, the upper ranges do overlap. Considering that the blood concentrations reported are postmortem, higher concentrations due to a large bolus dose of fentanyl cannot be ruled out. Therapeutic levels of fentanyl are complicated by tolerance with continued use. Hospital inpatients have demonstrated blood fentanyl concentrations up to 9.9 μg/l (29.42 nM) with chronic treatment (Thompson *et al.*, 2007). Additionally, blood fentanyl levels may not be a good indication of tissue levels as fentanyl undergoes extensive distribution. In fact, it has been reported that after an intravenous dose in rats, the concentrations of fentanyl in heart tissue are two to three times higher than plasma (Hug & Murphy, 1981). Thus, fentanyl may induce a high torsadogenic risk by blocking hERG channels, leading to sudden death, especially under the circumstances described below. First, chronic fentanyl users may experience periods of hypoxia as a result of respiratory depression (McQueen, 1983). Chronic hypoxia reduces mature hERG density and whole-cell current (Lamothe *et al.*, 2017). As I found that chronic hypoxia and fentanyl have an additive effect in decreasing I_{hERG} (Fig. 17), hERG block by fentanyl may pose a greater risk in the context of chronic respiratory depression. Second,

(Solis *et al.*, 2017) found that intravenous fentanyl causes a prolonged increase in temperature due to metabolic brain activation and skin vasoconstriction. Hyperthermia in the presence of I_{Kr} block increases the transmural dispersion of APD (Burashnikov *et al.*, 2008), which indicates a higher risk for arrhythmia (Surawicz, 1996). Fentanyl-mediated hERG blockade was analyzed at room temperature (22°C) in the present project. Although our analysis at physiologic temperature (37°C) did not alter fentanyl blocking potency (data not shown), the effects of increased temperature on transmural dispersion in the presence of fentanyl should not be ruled out. Third, conditions that cause alkalosis such as repetitive vomiting, severe dehydration, or endocrine disorders (Yee & Rabinstein, 2010) would potentiate block of hERG by fentanyl. Finally, hypokalemia is associated with an impairment of hERG function (Guo *et al.*, 2009; Massaeli *et al.*, 2010). Therefore, arrhythmia risk may be increased when fentanyl is used by those with existing electrolyte imbalances or when used concomitantly with other medications that interfere with hERG function.

In summary, we presented fentanyl as a hERG channel blocker that was capable of prolonging APD_{90}. We also demonstrated that fentanyl blocked hERG current in concentration-dependent, channel state–dependent, and voltage-dependent manners, whereas inactivation did not play a role. Naloxone did not block hERG at relevant concentrations, indicating that the observed arrhythmias may be due to the inciting drug or a separate mechanism. Although this project does not conclusively demonstrate that hERG block by fentanyl is responsible for fentanyl-related death, it provides an alternative molecular mechanism, especially for those individuals with overdoses or circumstances where hERG function is compromised (e.g., hypoxia, hypokalemia, other drugs).

Future Directions

A limitation of this work is the majority of experiments were performed in hERG 1a-expressing HEK cells. Although we showed that I_{Kr} recorded from NRVMs was also blocked by fentanyl, the IC_{50} or other properties of block were not determined in cardiomyocytes. Therefore, it would be beneficial to perform further experiments with cardiomyocytes to replicate our findings. Additionally, the hERG-HEK cell line used in this project lacks the hERG 1b isoform present *in vivo*. To this end, we co-expressed WT and Δ2-354 hERG to mimic hERG 1a/1b heterotetramers. However, Δ2-354 hERG is not equivalent to hERG 1b, as hERG 1b lacks the first 376 amino acids and contains a unique 36 amino acid N-terminal region (Fig. 2) (Lees-Miller *et al.*, 1997; London *et al.*, 1997). Further, it is unknown whether co-expression resulted in formation of heterotetramers or simply formation of separate WT and Δ2-354 hERG homotetramers. To address this, we have requested a stable, well characterized hERG 1a/b cell line from the laboratory of Gail Robertson (Ríos Pérez *et al.*, 2018).

Another finding that warrants further exploration is the extracellular pH-dependence of hERG block by fentanyl, as several possible explanations remain. To isolate the effects of fentanyl ionization state from extracellular pH, (±)-N-(3-fluoro-1-phenethylpiperidine-4-yl)-N-phenyl propionamide (NFEPP), also known as 3-flurofentanyl, could be used (Spahn *et al.*, 2017; Rodriguez-Gaztelumendi *et al.*, 2018). NFEPP has a pK_a of 6.8, meaning that it is mostly neutral at physiologic pH, in contrast to fentanyl, which is primarily positively charged. hERG block potency could be determined with NFEPP to examine the impact of the ionization state of fentanyl without altering extracellular pH.

Lastly, while we have demonstrated that fentanyl can prolong APD in isolated NRVMs, we have not demonstrated a direct link between hERG block by fentanyl and ventricular

arrhythmia. To address this, *in vivo* experiments could be performed using an animal model for drug-induced LQTS such as rabbit or guinea pig (Vargas *et al.*, 2015) to examine if fentanyl at clinically relevant doses prolongs the QT interval. Additionally, an observational study could be conducted in humans to monitor for QT prolongation in patients receiving fentanyl, or in patients admitted for fentanyl overdose. Such studies would be useful in determining if the hERG block we have demonstrated translates to LQTS and risk of arrhythmia *in vivo*.

Reference List

Abbott GW, Sesti F, Splawski I, Buck ME, Lehmann MH, Timothy KW, Keating MT & Goldstein SA (1999). MiRP1 forms I_{Kr} potassium channels with HERG and is associated with cardiac arrhythmia. *Cell* **97,** 175–187.

Abbott GW, Xu X & Roepke TK (2007). Impact of ancillary subunits on ventricular repolarization. *J Electrocardiol* **40,** S42–S46.

Akhavan A, Atanasiu R, Noguchi T, Han W, Holder N & Shrier A (2005). Identification of the cyclic-nucleotide-binding domain as a conserved determinant of ion-channel cell-surface localization. *J Cell Sci* **118,** 2803–2812.

Akhavan A, Atanasiu R & Shrier A (2003). Identification of a COOH-terminal Segment Involved in Maturation and Stability of Human Ether-a-go-go-related Gene Potassium Channels. *J Biol Chem* **278,** 40105–40112.

Anantharam A & Abbott GW (2005). Does hERG coassemble with a beta subunit? Evidence for roles of MinK and MiRP1. *Novartis Found Symp* **266,** 100–112; discussion 112-117, 155–158.

Andree RA (1980). Sudden Death following Naloxone Administration. *Anesth Analg* **59,** 782.

Anumonwo JM, Horta J, Delmar M, Taffet SM & Jalife J (1999). Proton and zinc effects on HERG currents. *Biophys J* **77,** 282–298.

Azar I & Turndorf H (1979). Severe hypertension and multiple atrial premature contractions following naloxone administration. *Anesth Analg* **58,** 524–525.

Barhanin J, Lesage F, Guillemare E, Fink M, Lazdunski M & Romey G (1996). K_VLQT1 and lsK (minK) proteins associate to form the I_{Ks} cardiac potassium current. *Nature* **384,** 78–80.

Baruscotti M, Bucchi A & DiFrancesco D (2005). Physiology and pharmacology of the cardiac pacemaker ("funny") current. *Pharmacol Ther* **107,** 59–79.

BC Coroners Service (2019). Fentanyl-detected illicit drug overdose deaths. Available at: https://www2.gov.bc.ca/assets/gov/birth-adoption-death-marriage-and-divorce/deaths/coroners-service/statistical/fentanyl-detected-overdose.pdf [Accessed April 25, 2019].

Behzadi M, Joukar S & Beik A (2018). Opioids and Cardiac Arrhythmia: A Literature Review. *Med Princ Pract Int J Kuwait Univ Health Sci Cent* **27,** 401–414.

Bett GCL & Rasmusson RL (2003). Functionally-distinct proton-binding in HERG suggests the presence of two binding sites. *Cell Biochem Biophys* **39,** 183–193.

Blair JR, Pruett JK, Introna RP, Adams RJ & Balser JS (1989). Cardiac electrophysiologic effects of fentanyl and sufentanil in canine cardiac Purkinje fibers. *Anesthesiology* **71,** 565–570.

Bovill JG & Sebel PS (1980). Pharmacokinetics of high-dose fentanyl. A study in patients undergoing cardiac surgery. *Br J Anaesth* **52,** 795–801.

Burashnikov A, Shimizu W & Antzelevitch C (2008). Fever accentuates transmural dispersion of repolarization and facilitates development of early afterdepolarizations and torsade de pointes under long-QT Conditions. *Circ Arrhythm Electrophysiol* **1,** 202–208.

Cabral JHM, Lee A, Cohen SL, Chait BT, Li M & Mackinnon R (1998). Crystal Structure and Functional Analysis of the HERG Potassium Channel N Terminus: A Eukaryotic PAS Domain. *Cell* **95,** 649–655.

Cafiero T, Di Minno RM & Di Iorio C (2011). QT interval and QT dispersion during the induction of anesthesia and tracheal intubation: a comparison of remifentanil and fentanyl. *Minerva Anestesiol* **77,** 160–165.

Chang DJ, Kweon TD, Nam SB, Lee JS, Shin CS, Park CH & Han DW (2008). Effects of fentanyl pretreatment on the QTc interval during propofol induction. *Anaesthesia* **63,** 1056–1060.

Chen J, Seebohm G & Sanguinetti MC (2002). Position of aromatic residues in the S6 domain, not inactivation, dictates cisapride sensitivity of HERG and eag potassium channels. *Proc Natl Acad Sci* **99,** 12461–12466.

Chiang C-E & Roden DM (2000). The long QT syndromes: genetic basis and clinical implications. *J Am Coll Cardiol* **36,** 1–12.

Cho JS, Kim SH, Shin S, Pak H-N, Yang SJ & Oh YJ (2016). Effects of Dexmedetomidine on Changes in Heart Rate Variability and Hemodynamics During Tracheal Intubation. *Am J Ther* **23,** e369-376.

Clark AK, Wilder CM & Winstanley EL (2014). A systematic review of community opioid overdose prevention and naloxone distribution programs. *J Addict Med* **8,** 153–163.

Curran ME, Splawski I, Timothy KW, Vincen GM, Green ED & Keating MT (1995). A molecular basis for cardiac arrhythmia: HERG mutations cause long QT syndrome. *Cell* **80,** 795–803.

Cuss FM, Colaço CB & Baron JH (1984). Cardiac arrest after reversal of effects of opiates with naloxone. *Br Med J Clin Res Ed* **288,** 363–364.

Deal KK, England SK & Tamkun MM (1996). Molecular physiology of cardiac potassium channels. *Physiol Rev* **76,** 49–67.

Ficker E, Jarolimek W, Kiehn J, Baumann A & Brown AM (1998). Molecular Determinants of Dofetilide Block of HERG K+ Channels. *Circ Res* **82,** 386–395.

Finley MR, Li Y, Hua F, Lillich J, Mitchell KE, Ganta S, Gilmour RF & Freeman LC (2002). Expression and coassociation of ERG1, KCNQ1, and KCNE1 potassium channel proteins in horse heart. *Am J Physiol-Heart Circ Physiol* **283,** H126–H138.

Gerlach AC, Stoehr SJ & Castle NA (2010). Pharmacological removal of human ether-à-go-go-related gene potassium channel inactivation by 3-nitro-N-(4-phenoxyphenyl) benzamide (ICA-105574). *Mol Pharmacol* **77,** 58–68.

Goromaru T, Matsuura H, Yoshimura N, Miyawaki T, Sameshima T, Miyao J, Furuta T & Baba S (1984). Identification and Quantitative Determination of Fentanyl Metabolites in Patients by Gas Chromatography-Mass Spectrometry. *Anesthesiol J Am Soc Anesthesiol* **61,** 73–77.

Grilo LS, Carrupt P-A & Abriel H (2010). Stereoselective Inhibition of the hERG1 Potassium Channel. *Front Pharmacol*; DOI: 10.3389/fphar.2010.00137.

Guo J, Gang H & Zhang S (2006). Molecular Determinants of Cocaine Block of Human Ether-á-go-go-Related Gene Potassium Channels. *J Pharmacol Exp Ther* **317,** 865–874.

Guo J, Massaeli H, Li W, Xu J, Luo T, Shaw J, Kirshenbaum LA & Zhang S (2007). Identification of I_{Kr} and Its Trafficking Disruption Induced by Probucol in Cultured Neonatal Rat Cardiomyocytes. *J Pharmacol Exp Ther* **321,** 911–920.

Guo J, Massaeli H, Xu J, Jia Z, Wigle JT, Mesaeli N & Zhang S (2009). Extracellular K^+ concentration controls cell surface density of I_{Kr} in rabbit hearts and of the HERG channel in human cell lines. *J Clin Invest* **119,** 2745–2757.

Gustina AS & Trudeau MC (2011). hERG potassium channel gating is mediated by N- and C-terminal region interactions. *J Gen Physiol* **137,** 315–325.

Hancı V, Yurtlu S, Karabağ T, Okyay D, Hakimoğlu S, Kayhan G, Büyükuysal Ç, Ayoğlu H & Özkoçak Turan I (2013). Effects of esmolol, lidocaine and fentanyl on P wave dispersion, QT, QTc intervals and hemodynamic responses to endotracheal intubation during propofol induction: a comparative study. *Braz J Anesthesiol Elsevier* **63,** 235–244.

Hug CC & Murphy MR (1979). Fentanyl Disposition in Cerebrospinal Fluid and Plasma and Its Relationship to Ventilatory Depression in the Dog. *Anesthesiol J Am Soc Anesthesiol* **50,** 342–349.

Hug CC & Murphy MR (1981). Tissue redistribution of fentanyl and termination of its effects in rats. *Anesthesiology* **55,** 369–375.

Hunter R (2005). Ventricular tachycardia following naloxone administration in an illicit drug misuse. *J Clin Forensic Med* **12,** 218–219.

Jenke M, Sánchez A, Monje F, Stühmer W, Weseloh RM & Pardo LA (2003). C-terminal domains implicated in the functional surface expression of potassium channels. *EMBO J* **22,** 395–403.

Jiang M, Dun W & Tseng G-N (1999). Mechanism for the effects of extracellular acidification on HERG-channel function. *Am J Physiol-Heart Circ Physiol* **277,** H1283–H1292.

Jones DK, Liu F, Vaidyanathan R, Eckhardt LL, Trudeau MC & Robertson GA (2014). hERG 1b is critical for human cardiac repolarization. *Proc Natl Acad Sci U S A* **111,** 18073–18077.

Jones EMC, Roti ECR, Wang J, Delfosse SA & Robertson GA (2004). Cardiac I_{Kr} Channels Minimally Comprise hERG 1a and 1b Subunits. *J Biol Chem* **279,** 44690–44694.

Kalyaanamoorthy S & Barakat KH (2018). Development of Safe Drugs: The hERG Challenge. *Med Res Rev* **38,** 525–555.

Katchman AN, McGroary KA, Kilborn MJ, Kornick CA, Manfredi PL, Woosley RL & Ebert SN (2002). Influence of opioid agonists on cardiac human ether-a-go-go-related gene K^+ currents. *J Pharmacol Exp Ther* **303,** 688–694.

Keating MT & Sanguinetti MC (2001). Molecular and cellular mechanisms of cardiac arrhythmias. *Cell* **104,** 569–580.

Keller GA, Alvarez PA, Ponte ML, Belloso WH, Bagnes C, Sparanochia C, Gonzalez CD, Villa Etchegoyen MC, Diez RA & Di Girolamo G (2016). Drug-Induced QTc Interval Prolongation: A Multicenter Study to Detect Drugs and Clinical Factors Involved in Every Day Practice. *Curr Drug Saf* **11,** 86–98.

Kim H-J, Litzenburger BC, Cui X, Delgado DA, Grabiner BC, Lin X, Lewis MT, Gottardis MM, Wong TW, Attar RM, Carboni JM & Lee AV (2007). Constitutively active type I insulin-like growth factor receptor causes transformation and xenograft growth of immortalized mammary epithelial cells and is accompanied by an epithelial-to-mesenchymal transition mediated by NF-kappaB and snail. *Mol Cell Biol* **27,** 3165–3175.

Lameijer H, Azizi N, Ligtenberg JJM & Ter Maaten JC (2014). Ventricular Tachycardia After Naloxone Administration: a Drug Related Complication? Case Report and Literature Review. *Drug Saf - Case Rep*; DOI: 10.1007/s40800-014-0002-0.

Lamothe SM, Song W, Guo J, Li W, Yang T, Baranchuk A, Graham CH & Zhang S (2017). Hypoxia reduces mature hERG channels through calpain up-regulation. *FASEB J* **31,** 5068–5077.

Larsen AP & Olesen S-P (2010). Differential expression of hERG1 channel isoforms reproduces properties of native I_{Kr} and modulates cardiac action potential characteristics. *PloS One* **5,** e9021.

Lees-Miller JP, Duan Y, Teng GQ & Duff HJ (2000). Molecular Determinant of High-Affinity Dofetilide Binding toHERG1 Expressed in Xenopus Oocytes: Involvement of S6 Sites. *Mol Pharmacol* **57,** 367–374.

Lees-Miller JP, Kondo C, Wang L & Duff HJ (1997). Electrophysiological characterization of an alternatively processed ERG K^+ channel in mouse and human hearts. *Circ Res* **81,** 719–726.

Li Y, Um SY & Mcdonald TV (2006). Voltage-Gated Potassium Channels: Regulation by Accessory Subunits. *The Neuroscientist* **12,** 199–210.

Lischke V, Wilke HJ, Probst S, Behne M & Kessler P (1994). Prolongation of the QT-interval during induction of anesthesia in patients with coronary artery disease. *Acta Anaesthesiol Scand* **38,** 144–148.

London B, Trudeau MC, Newton KP, Beyer AK, Copeland NG, Gilbert DJ, Jenkins NA, Satler CA & Robertson GA (1997). Two isoforms of the mouse ether-a-go-go-related gene coassemble to form channels with properties similar to the rapidly activating component of the cardiac delayed rectifier K+ current. *Circ Res* **81,** 870–878.

Luckenbill K, Thompson J, Middleton O, Kloss J & Apple F (2008). Fentanyl Postmortem Redistribution: Preliminary Findings Regarding the Relationship Among Femoral Blood and Liver and Heart Tissue Concentrations. *J Anal Toxicol* **32,** 639–643.

Maguire P, Tsai N, Kamal J, Cometta-Morini C, Upton C & Loew G (1992). Pharmacological profiles of fentanyl analogs at μ, δ and κ opiate receptors. *Eur J Pharmacol* **213,** 219–225.

Martin TL, Woodall KL & McLellan BA (2006). Fentanyl-related deaths in Ontario, Canada: toxicological findings and circumstances of death in 112 cases (2002-2004). *J Anal Toxicol* **30,** 603–610.

Martin WR (1976). Naloxone. *Ann Intern Med* **85,** 765–768.

Massaeli H, Guo J, Xu J & Zhang S (2010). Extracellular K^+ is a prerequisite for the function and plasma membrane stability of HERG channels. *Circ Res* **106,** 1072–1082.

Mazhari R, Greenstein JL, Winslow RL, Marbán E & Nuss HB (2001). Molecular interactions between two long-QT syndrome gene products, HERG and KCNE2, rationalized by in vitro and in silico analysis. *Circ Res* **89,** 33–38.

McClain DA & Hug CC (1980). Intravenous fentanyl kinetics. *Clin Pharmacol Ther* **28,** 106–114.

McDonald TV, Yu Z, Ming Z, Palma E, Meyers MB, Wang K-W, Goldstein SAN & Fishman GI (1997). A minK–HERG complex regulates the cardiac potassium current I_{Kr}. *Nature* **388,** 289.

McQueen DS (1983). Opioid peptide interactions with respiratory and circulatory systems. *Br Med Bull* **39,** 77–82.

Merigian KS (1993). Cocaine-induced ventricular arrhythmias and rapid atrial fibrillation temporally related to naloxone administration. *Am J Emerg Med* **11,** 96–97.

Michaelis LL, Hickey PR, Clark TA & Dixon WM (1974). Ventricular irritability associated with the use of naloxone hydrochloride. Two case reports and laboratory assessment of the effect of the drug on cardiac excitability. *Ann Thorac Surg* **18,** 608–614.

Mitcheson JS, Chen J, Lin M, Culberson C & Sanguinetti MC (2000*a*). A structural basis for drug-induced long QT syndrome. *Proc Natl Acad Sci* **97,** 12329–12333.

Mitcheson JS, Chen J & Sanguinetti MC (2000*b*). Trapping of a Methanesulfonanilide by Closure of the Herg Potassium Channel Activation Gate. *J Gen Physiol* **115,** 229–240.

Mitcheson JS & Hancox JC (1999). An investigation of the role played by the E-4031-sensitive (rapid delayed rectifier) potassium current in isolated rabbit atrioventricular nodal and ventricular myocytes. *Pflugers Arch* **438,** 843–850.

Moreno C, Macias A, Prieto A, de la Cruz A, Gonzalez T & Valenzuela C (2012). Effects of n−3 Polyunsaturated Fatty Acids on Cardiac Ion Channels. *Front Physiol*; DOI: 10.3389/fphys.2012.00245.

Murphy MR, Olson WA & Hug CC (1979). Pharmacokinetics of 3H-fentanyl in the dog anesthetized with enflurane. *Anesthesiology* **50,** 13–19.

Ng CA, Hunter MJ, Perry MD, Mobli M, Ke Y, Kuchel PW, King GF, Stock D & Vandenberg JI (2011). The N–Terminal Tail of hERG Contains an Amphipathic α–Helix That Regulates Channel Deactivation. *PLOS ONE* **6,** e16191.

Ng CA, Phan K, Hill AP, Vandenberg JI & Perry MD (2014). Multiple Interactions between Cytoplasmic Domains Regulate Slow Deactivation of Kv11.1 Channels. *J Biol Chem* **289,** 25822–25832.

Olson KN, Luckenbill K, Thompson J, Middleton O, Geiselhart R, Mills KM, Kloss J & Apple FS (2010). Postmortem Redistribution of Fentanyl in Blood. *Am J Clin Pathol* **133,** 447–453.

Öztürk T, Ağdanli D, Bayturan Ö, Çikrikci C & Keleş GT (2015). Effects of conventional vs high-dose rocuronium on the QTc interval during anesthesia induction and intubation in patients undergoing coronary artery surgery: a randomized, double-blind, parallel trial. *Braz J Med Biol Res Rev Bras Pesqui Medicas E Biol* **48,** 370–376.

Perrin MJ, Subbiah RN, Vandenberg JI & Hill AP (2008). Human ether-a-go-go related gene (hERG) K^+ channels: function and dysfunction. *Prog Biophys Mol Biol* **98,** 137–148.

Perry M, Groot MJ de, Helliwell R, Leishman D, Tristani-Firouzi M, Sanguinetti MC & Mitcheson J (2004). Structural Determinants of HERG Channel Block by Clofilium and Ibutilide. *Mol Pharmacol* **66,** 240–249.

Phartiyal P, Jones EMC & Robertson GA (2007). Heteromeric Assembly of Human Ether-à-go-go-related Gene (hERG) 1a/1b Channels Occurs Cotranslationally via N-terminal Interactions. *J Biol Chem* **282,** 9874–9882.

Raynor K, Kong H, Chen Y, Yasuda K, Yu L, Bell GI & Reisine T (1994). Pharmacological characterization of the cloned kappa-, delta-, and mu-opioid receptors. *Mol Pharmacol* **45,** 330–334.

Ríos Pérez EB, Liu F, Stevens-Sostre W & Robertson GA (2018). A Novel hERG 1a/1b Stable Cell Line for Drug Screening and Research Applications. *Biophys J* **114,** 292a.

Roden DM (2004). Drug-Induced Prolongation of the QT Interval. *N Engl J Med* **350,** 1013–1022.

Rodriguez-Gaztelumendi A, Spahn V, Labuz D, Machelska H & Stein C (2018). Analgesic effects of a novel pH-dependent μ-opioid receptor agonist in models of neuropathic and abdominal pain. *Pain* **159,** 2277–2284.

Rzasa Lynn R & Galinkin J (2018). Naloxone dosage for opioid reversal: current evidence and clinical implications. *Ther Adv Drug Saf* **9,** 63–88.

Sale H, Wang J, O'Hara TJ, Tester DJ, Phartiyal P, He J-Q, Rudy Y, Ackerman MJ & Robertson GA (2008). Physiological Properties of hERG 1a/1b Heteromeric Currents and a hERG 1b-specific Mutation Associated with Long QT Syndrome. *Circ Res* **103,** e81–e95.

Sanguinetti MC, Curran ME, Zou A, Shen J, Spector PS, Atkinson DL & Keating MT (1996). Coassembly of K_VLQT1 and minK (IsK) proteins to form cardiac I_{Ks} potassium channel. *Nature* **384,** 80–83.

Sanguinetti MC, Jiang C, Curran ME & Keating MT (1995). A mechanistic link between an inherited and an acquired cardiac arrhythmia: HERG encodes the I_{Kr} potassium channel. *Cell* **81,** 299–307.

Sanguinetti MC & Jurkiewicz NK (1990). Two components of cardiac delayed rectifier K^+ current. Differential sensitivity to block by class III antiarrhythmic agents. *J Gen Physiol* **96,** 195–215.

Schneider E & Brune K (1986). Opioid activity and distribution of fentanyl metabolites. *Naunyn Schmiedebergs Arch Pharmacol* **334,** 267–274.

Schönherr R & Heinemann SH (1996). Molecular determinants for activation and inactivation of HERG, a human inward rectifier potassium channel. *J Physiol* **493 (Pt 3),** 635–642.

Shimizu W, Ohe T, Kurita T, Kawade M, Arakaki Y, Aihara N, Kamakura S, Kamiya T & Shimomura K (1995). Effects of verapamil and propranolol on early afterdepolarizations and ventricular arrhythmias induced by epinephrine in congenital long QT syndrome. *J Am Coll Cardiol* **26,** 1299–1309.

Skomedal H, Kristensen GB, Nesland JM, Børresen-Dale AL, Tropé C & Holm R (1999). TP53 alterations in relation to the cell cycle-associated proteins p21, cyclin D1, CDK4, RB, MDM2, and EGFR in cancers of the uterine corpus. *J Pathol* **187,** 556–562.

Smith PL, Baukrowitz T & Yellen G (1996). The inward rectification mechanism of the HERG cardiac potassium channel. *Nature* **379,** 833–836.

Solis E, Cameron-Burr KT & Kiyatkin EA (2017). Heroin Contaminated with Fentanyl Dramatically Enhances Brain Hypoxia and Induces Brain Hypothermia. *eNeuro*; DOI: 10.1523/ENEURO.0323-17.2017.

Spahn V, Vecchio GD, Labuz D, Rodriguez-Gaztelumendi A, Massaly N, Temp J, Durmaz V, Sabri P, Reidelbach M, Machelska H, Weber M & Stein C (2017). A nontoxic pain killer designed by modeling of pathological receptor conformations. *Science* **355,** 966–969.

Spector PS, Curran ME, Keating MT & Sanguinetti MC (1996*a*). Class III antiarrhythmic drugs block HERG, a human cardiac delayed rectifier K^+ channel. Open-channel block by methanesulfonanilides. *Circ Res* **78,** 499–503.

Spector PS, Curran ME, Zou A, Keating MT & Sanguinetti MC (1996*b*). Fast inactivation causes rectification of the I_{Kr} channel. *J Gen Physiol* **107,** 611–619.

Stanley TH (2014). The Fentanyl Story. *J Pain* **15,** 1215–1226.

Stork D, Timin EN, Berjukow S, Huber C, Hohaus A, Auer M & Hering S (2007). State dependent dissociation of HERG channel inhibitors. *Br J Pharmacol* **151,** 1368–1376.

Streisand JB, Zhang J, Niu S, McJames S, Natte R & Pace NL (1995). Buccal absorption of fentanyl is pH-dependent in dogs. *Anesthesiology* **82,** 759–764.

Surawicz B (1996). Will QT dispersion play a role in clinical decision-making? *J Cardiovasc Electrophysiol* **7,** 777–784.

Tanaka N, Naito T, Yagi T, Doi M, Sato S & Kawakami J (2014). Impact of CYP3A5*3 on Plasma Exposure and Urinary Excretion of Fentanyl and Norfentanyl in the Early Postsurgical Period. *Ther Drug Monit* **36,** 345–352.

Tateishi T, Krivoruk Y, Ueng YF, Wood AJ, Guengerich FP & Wood M (1996). Identification of human liver cytochrome P-450 3A4 as the enzyme responsible for fentanyl and sufentanil N-dealkylation. *Anesth Analg* **82,** 167–172.

Terai T, Furukawa T, Katayama Y & Hiraoka M (2000). Effects of external acidosis on HERG current expressed in Xenopus oocytes. *J Mol Cell Cardiol* **32,** 11–21.

Thompson JG, Baker AM, Bracey AH, Seningen J, Kloss JS, Strobl AQ & Apple FS (2007). Fentanyl concentrations in 23 postmortem cases from the hennepin county medical examiner's office. *J Forensic Sci* **52,** 978–981.

Thurlkill RL, Cross DA, Scholtz JM & Pace CN (2005). pKa of fentanyl varies with temperature: implications for acid-base management during extremes of body temperature. *J Cardiothorac Vasc Anesth* **19,** 759–762.

Trudeau MC, Warmke JW, Ganetzky B & Robertson GA (1995). HERG, a human inward rectifier in the voltage-gated potassium channel family. *Science* **269,** 92–95.

Tschirhart JN, Li W, Guo J & Zhang S (2019). Blockade of the Human Ether A-Go-Go–Related Gene (hERG) Potassium Channel by Fentanyl. *Mol Pharmacol* **95,** 386–397.

Van Rooy HH, Vermeulen MP & Bovill JG (1981). The assay of fentanyl and its metabolites in plasma of patients using gas chromatography with alkali flame ionisation detection and gas chromatography-mass spectrometry. *J Chromatogr* **223,** 85–93.

Van Slyke AC, Cheng YM, Mafi P, Allard CR, Hull CM, Shi YP & Claydon TW (2012). Proton block of the pore underlies the inhibition of hERG cardiac K^+ channels during acidosis. *Am J Physiol-Cell Physiol* **302,** C1797–C1806.

Vandenberg JI, Perry MD, Perrin MJ, Mann SA, Ke Y & Hill AP (2012). hERG K^+ Channels: Structure, Function, and Clinical Significance. *Physiol Rev* **92,** 1393–1478.

Vandenberg JI, Varghese A, Lu Y, Bursill JA, Mahaut-Smith MP & Huang CL-H (2006). Temperature dependence of human ether-a-go-go-related gene K^+ currents. *Am J Physiol Cell Physiol* **291,** C165-175.

Vargas HM, Bass AS, Koerner J, Matis-Mitchell S, Pugsley MK, Skinner M, Burnham M, Bridgland-Taylor M, Pettit S & Valentin J-P (2015). Evaluation of drug-induced QT interval prolongation in animal and human studies: a literature review of concordance. *Br J Pharmacol* **172,** 4002–4011.

Villiger JW, Ray LJ & Taylor KM (1983). Characteristics of [3H]fentanyl binding to the opiate receptor. *Neuropharmacology* **22,** 447–452.

Viloria CG, Barros F, Giráldez T, Gómez-Varela D & de la Peña P (2000). Differential effects of amino-terminal distal and proximal domains in the regulation of human erg K^+ channel gating. *Biophys J* **79,** 231–246.

Walker BD, Singleton CB, Bursill JA, Wyse KR, Valenzuela SM, Qiu MR, Breit SN & Campbell TJ (1999). Inhibition of the human ether-a-go-go-related gene (HERG) potassium channel by cisapride: affinity for open and inactivated states. *Br J Pharmacol* **128,** 444–450.

Wamsley JK (1983). Opioid receptors: autoradiography. *Pharmacol Rev* **35,** 69–83.

Wang J, Trudeau MC, Zappia AM & Robertson GA (1998). Regulation of Deactivation by an Amino Terminal Domain in Human Ether-à-go-go –related Gene Potassium Channels. *J Gen Physiol* **112,** 637–647.

Wang S, Morales MJ, Liu S, Strauss HC & Rasmusson RL (1997). Modulation of HERG affinity for E-4031 by $[K^+]_o$ and C-type inactivation. *FEBS Lett* **417,** 43–47.

Wang W & MacKinnon R (2017). Cryo-EM Structure of the Open Human Ether-à-go-go-Related K^+ Channel hERG. *Cell* **169,** 422-430.e10.

Warmke JW & Ganetzky B (1994). A family of potassium channel genes related to eag in Drosophila and mammals. *Proc Natl Acad Sci U S A* **91,** 3438–3442.

Weerapura M, Nattel S, Chartier D, Caballero R & Hébert TE (2002). A comparison of currents carried by HERG, with and without coexpression of MiRP1, and the native rapid delayed rectifier current. Is MiRP1 the missing link? *J Physiol* **540,** 15–27.

Witchel HJ, Dempsey CE, Sessions RB, Perry M, Milnes JT, Hancox JC & Mitcheson JS (2004). The Low-Potency, Voltage-Dependent HERG Blocker Propafenone—Molecular Determinants and Drug Trapping. *Mol Pharmacol* **66,** 1201–1212.

Wu W, Gardner A & Sanguinetti MC (2015). The Link between Inactivation and High-Affinity Block of hERG1 Channels. *Mol Pharmacol* **87,** 1042–1050.

Xuan C, Wu N, Li Y, Sun X, Zhang Q & Ma H (2018). Corrected QT interval prolongation during anesthetic induction for laryngeal mask airway insertion with or without cisatracurium. *J Int Med Res* **46,** 1990–2000.

Yee AH & Rabinstein AA (2010). Neurologic Presentations of Acid-Base Imbalance, Electrolyte Abnormalities, and Endocrine Emergencies. *Neurol Clin* **28,** 1–16.

Zhang C, Zhang M-X, Shen YH, Burks JK, Li X-N, LeMaire SA, Yoshimura K, Aoki H, Matsuzaki M, An F-S, Engler DA, Matsunami RK, Coselli JS, Zhang Y & Wang XL (2008). Role of NonO-histone interaction in TNFalpha-suppressed prolyl-4-hydroxylase alpha1. *Biochim Biophys Acta* **1783,** 1517–1528.

Zhang S, Zhou Z, Gong Q, Makielski JC & January CT (1999). Mechanism of block and identification of the verapamil binding domain to HERG potassium channels. *Circ Res* **84,** 989–998.

Zhou Z, Gong Q, Ye B, Fan Z, Makielski JC, Robertson GA & January CT (1998). Properties of HERG Channels Stably Expressed in HEK 293 Cells Studied at Physiological Temperature. *Biophys J* **74,** 230–241.

Zhou Z, Vorperian VR, Gong Q, Zhang S & January CT (1999). Block of HERG potassium channels by the antihistamine astemizole and its metabolites desmethylastemizole and norastemizole. *J Cardiovasc Electrophysiol* **10,** 836–843.

Zou A, Xu QP & Sanguinetti MC (1998). A mutation in the pore region of HERG K^+ channels expressed in Xenopus oocytes reduces rectification by shifting the voltage dependence of inactivation. *J Physiol* **509 (Pt 1),** 129–137.